AD NUMBER

AD901852

LIMITATION CHANGES

TO:

Approved for public release; distribution is unlimited.

FROM:

Distribution authorized to U.S. Gov't. agencies only; Proprietary Information; JUL 1972. Other requests shall be referred to Arnold Engineering Development Center, Arnold AFB, TN.

AUTHORITY

AFAL per ltr, 16 Dec 1975

AEDC-TR-72-106
AFATL-TR-72-138

cy 2

TRANSONIC AERODYNAMIC CHARACTERISTICS OF BOMBLET MUNITION MODELS USED IN THE EVALUATION OF THE ROLL-THROUGH-ZERO AERODYNAMIC DISPERSION TECHNIQUE

T. O. Shadow and G. R. Gomillion

ARO, Inc.

July 1972

PROPULSION WIND TUNNEL FACILITY
ARNOLD ENGINEERING DEVELOPMENT CENTER
AIR FORCE SYSTEMS COMMAND
ARNOLD AIR FORCE STATION, TENNESSEE

NOTICES

When U. S. Government drawings specifications, or other data are used for any purpose other than a definitely related Government procurement operation, the Government thereby incurs no responsibility nor any obligation whatsoever, and the fact that the Government may have formulated, furnished, or in any way supplied the said drawings, specifications, or other data, is not to be regarded by implication or otherwise, or in any manner licensing the holder or any other person or corporation, or conveying any rights or permission to manufacture, use, or sell any patented invention that may in any way be related thereto.

Qualified users may obtain copies of this report from the Defense Documentation Center.

References to named commercial products in this report are not to be considered in any sense as an endorsement of the product by the United States Air Force or the Government.

TRANSONIC AERODYNAMIC CHARACTERISTICS OF BOMBLET MUNITION MODELS USED IN THE EVALUATION OF THE ROLL-THROUGH-ZERO AERODYNAMIC DISPERSION TECHNIQUE

T. O. Shadow and G. R. Gomillion
ARO, Inc.

FOREWORD

The work reported herein was sponsored by the Air Force Armament Laboratory (DLDL/M. J. Bouffard) Air Force Systems Command (AFSC), under Program Element 62602F, Project 2547.

The test results presented were obtained by ARO, Inc. (a subsidiary of Sverdrup & Parcel and Associates, Inc.), contract operator of the Arnold Engineering Development Center (AEDC), AFSC, Arnold Air Force Station, Tennessee, under Contract F40600-73-C-0004. The test was conducted in three phases from January 4 to April 20, 1972, under ARO Project No. PC0212. The manuscript was submitted for publication on June 15, 1972.

This technical report has been reviewed and is approved.

R. W. WORKING
Major, USAF
Chief Air Force Test Director, PWT
Directorate of Test

A. L. COAPMAN
Colonel, USAF
Director of Test

ABSTRACT

A wind-tunnel investigation was conducted in the Aerodynamic Wind Tunnel (4T) to determine the aerodynamic characteristics of bomblet munition models designed for the evaluation of the Roll-Through-Zero Aerodynamic Dispersal Technique. Static stability, pitch-damping, roll-damping, and magnus data were obtained at Mach numbers from 0.3 to 1.2 and angles of attack from zero to 24 deg at a constant Reynolds number of 2.2 x 10^6 based on the model length. Roll angle was varied from -165 to 180 deg for the static stability phase.

CONTENTS

APPENDIXES

I. ILLUSTRATIONS

Figure

NOMENCLATURE

C_A	Axial-force coefficient, measured axial force/$q_\infty S$
C_ℓ	Rolling-moment coefficient, measured rolling moment/$q_\infty Sd$
C_{ℓ_p}	Rolling-damping coefficient, $\partial C_\ell / \partial (pd/2V_\infty)$, per radian
C_{ℓ_δ}	Roll-driving-moment derivative coefficient, $\partial C_\ell / \partial \delta$, per degree
C_m	Pitching-moment coefficient (see Fig. 2 for moment reference location), measured pitching moment/$q_\infty Sd$
C_{m_q}, $C_{m_{\dot{\alpha}}}$	$\partial C_m / \partial (qd/2V_\infty)$, $\partial C_m / \partial (\dot{\alpha} d/2V_\infty)$ — Damping-in-pitch derivatives, per radian
C_N	Normal-force coefficient, measured normal force/$q_\infty S$
C_n	Yawing- or magnus-moment coefficient (see Fig. 2 for moment reference location) measured yawing moment/$q_\infty Sd$
C_{n_p}	Magnus-moment derivative coefficient, $\partial C_n / \partial (pd/2V_\infty)$
C_Y	Side- or magnus-force coefficient, measured side force/$q_\infty S$
C_{Y_p}	Magnus-force derivative coefficient, $\partial C_Y / \partial (pd/2V_\infty)$, per radian
d	Model body diameter (reference diameter), 0.2500 ft
h	Fin height, in.
I_x	Model mass moment of inertia about spin axis, ft-lb-sec^2

M	Moment, ft-lb
M_q	Pitch-damping-moment derivative, $\partial M/\partial q$, ft-lb-sec/radian
M_∞	Free-stream Mach number
p	Model spin rate (positive clockwise viewing from base), radians/sec
$pd/2V_\infty$	Peripheral speed ratio, radians
q	Pitching velocity, radians/sec
q_∞	Free-stream dynamic pressure, psf
S	Model cross-sectional area (reference area), 0.0491 sq ft
t	Time, sec
V_∞	Free-stream velocity, ft/sec
α	Model angle of attack with respect to tunnel centerline, deg
$\dot{\alpha}$	Time rate of change of angle of attack, radians/sec
δ_F	Fin incidence angle, deg
ϕ	Model roll angle, deg
ω	Angular frequency, radians/sec
$\omega d/2V_\infty$	Reduced frequency parameter, radian

SUBSCRIPTS

1,2	Successive data points
A	Autorotational conditions
a	Aerodynamic contribution
F_A, F_N	Attributable to axial and normal force
t	Tare contribution
v	Vacuum conditions
w	Wind-on conditions
x	Spin axis

MODEL NOMENCLATURE

A_{S1}	Cylindrical afterbody
A_{S2}	Boattail afterbody
B_S	Cylindrical centerbody, d = 0.2500 ft, S = 0.0491 sq ft
$F_{S2,5}$	Rectangular fins; 2 and 5 for 0.233- and 0.420-in. fin heights, respectively
N_{S2}	Spherical nose, 1.500-in. spherical radius

SECTION I
INTRODUCTION

A wind-tunnel investigation of bomblet munition models was conducted in the Aerodynamic Wind Tunnel (4T), Propulsion Wind Tunnel Facility (PWT), to determine the aerodynamic characteristics for use in the evaluation of the Roll-Through-Zero Aerodynamic Dispersal Technique. The tests were conducted at Mach numbers from 0.3 to 1.2 at a constant Reynolds number of 2.2×10^6 based on the model length.

With the Roll-Through-Zero concept, aerodynamic dispersion is achieved by a body-fixed trim lift. This lift force is randomly oriented about the flight path except during the period the bomblet is intentionally made to roll through zero angular velocity. During this period the lift force is predominantly in one quadrant, and effective dispersion is achieved.

Bomblets dispersed in this mode are susceptible to roll lock-in, since the spin rate must be varied over a wide range and could possibly include the aerodynamic pitch frequency. Basically, roll lock-in may occur when the roll rate is the same as the pitch rate. At this condition the roll frequency may lock onto the pitch frequency which results in a lunar motion. The pitch motion is amplified and thereby causes erroneous dispersion and possible destruction of the bomblet. This phenomenon has been investigated in many reports considering mass and aerodynamic asymmetries of ballistic-type reentry bodies and spinning sounding rockets.

Previous investigations of the Roll-Through-Zero Dispersal Technique were reported in Refs. 1 through 5. The configuration investigated, which consisted of an ellipsoid-cylinder-boattail body and cruciform blunt-nose, wedge fins exhibited a catastrophic roll lock-in which could not be eliminated through configuration redesign.

The present investigation expands on the knowledge gained in the previous investigations with the application of the Roll-Through-Zero Dispersal Technique to bomblets which exhibit S-shaped pitching-moment curves. The basic aerodynamic characteristics of this type configuration were also investigated in Refs. 1 through 5 and in Ref. 6.

SECTION II
APPARATUS

2.1 TEST FACILITY

The Aerodynamic Wind Tunnel (4T) is a closed-loop, continuous flow, variable-density tunnel in which the Mach number can be varied from 0.1 to 1.3. At all Mach numbers, the stagnation pressure can be varied from 300 to 3700 psfa. The test section is 4 ft square and 12.5 ft long with perforated, variable porosity (0.5- to 10-percent-open) walls. It is completely enclosed in a plenum chamber from which the air can be evacuated, allowing part of the tunnel airflow to be removed through the perforated walls of the test section. A more thorough description of the tunnel is given in Ref. 7.

The model support system consists of a pitch sector, boom, and sting which provide a pitch capability from -12 to 28 deg with respect to the tunnel centerline. The center of rotation is at tunnel station 108. In addition, a remote-controlled roll mechanism allows roll angle variations of ±180 deg. Schematics and photographs of the test installations for the three phases are shown in Fig. 1 (Appendix I).

2.2 TEST ARTICLES AND TEST MECHANISMS

Details of the bomblet models used in the three test phases are shown in Fig. 2. The basic model consisted of a 3-in.-diam cylindrical centerbody and afterbody and a spherical nose. Configuration variables consisted of (1) straight or boattail afterbody, (2) fin height, and (3) fin incidence.

For the static stability phase, two of the six fins were rotated about their midpoint to produce 10-deg incidence relative to the model centerline in the pitch plane (Fig. 2a). Fin height was the configuration variable.

The basic model with straight afterbody and the largest fin span was used in the pitch-damping phase (Fig. 2b).

In the roll dynamics phase all six fins were rotated about their midpoint to produce 3-deg incidence relative to the model centerline. Configuration variables consisted of fin incidence and straight and boattail afterbody (Fig. 2c).

Pitch-damping data were obtained with a small amplitude (±3 deg), forced-oscillation balance system (Ref. 8) which is a one-degree-of-freedom oscillatory system incorporating a cross-flexure pivot (Fig. 3a). During the test, model oscillation amplitudes were approximately ±1.8 deg. The balance was forced to oscillate by an electromagnetic shaker motor located in the aft portion of the sting.

The roll dynamics test mechanism (Fig. 3b) consists of a sting-mounted six-component balance connected to the model through an adapter which allows free rotation of the model on ball bearings about its longitudinal axis. A hydraulic motor-driven shaft, which rotates outside the sting, is used along with a pneumatic air-operated clutch to prespin the model to a specified spin rate. The clutch can be disengaged quickly to allow free decay to zero spin rate.

2.3 INSTRUMENTATION

An internal six-component strain-gage balance was used during the static stability and roll dynamics phase to measure forces and moments on the model. During the static stability phase, differential pressure transducers, referenced to the tunnel plenum pressure were used to measure the pressure at the base of the models. A photocell pickup was used to measure rotational velocity for the roll-damping and magnus measurements. The pickup, which included both light source and receiver, was mounted on the stationary adapter (Fig. 3b) and was triggered when reflecting surfaces from gear teeth located on the rotating adapter returned the light to the receiver.

Angular displacement of the model during the pitch-damping phase was measured by a strain-gage bridge mounted on a cross flexure, and the input torque to the system was measured by a strain-gage bridge mounted at the minimum cross-sectional area of the torque beam. When the model balance system was oscillated at a frequency other than its undamped natural frequency, electronic resolvers were used to determine the in-phase and out-of-phase components of the forcing torque signal. The forcing system is equipped with a feedback control network as described in Ref. 8 to provide positive amplitude control for testing either dynamically stable or unstable configurations.

Electrical signals from the balances, photocell pickup and standard tunnel instrumentation systems were processed by the PWT data acquisition system and digital computer for on-line data reduction.

SECTION III
TEST DESCRIPTION

3.1 TEST CONDITIONS AND PROCEDURES

Data were obtained at nominal Mach numbers from 0.3 to 1.2. Stagnation temperature was maintained at approximately 100°F throughout the test. A summary of test conditions is given in Tables I through III (Appendix II). Free transition was used throughout the test.

Pitch-damping data were recorded by oscillating the model at approximately ±1.8 deg and recording the resulting time-resolved torque signal, in-phase and out-of-phase components of the torque signal, and displacement signal, which had been converted to d-c levels, over a set time period (nominally 10 sec).

Roll-damping and magnus data were recorded with the model spin rate decaying or increasing, depending on the model fin incidence. With fin incidence at zero, the model was prespun to a set spin rate. Then, the clutch was disengaged, and six-component balance data and spin rate were recorded as the model spin rate decayed to zero. When fin incidence was not zero, the model was released and data were recorded as model spin rate increased to the autorotational spin rate.

3.2 DATA REDUCTION

The balance forces and moments for the static stability phase were reduced to aerodynamic coefficients in the nonrolling body-axis coordinate system with the moment reference point 1.5 cal from the nose of the model.

Pitch-damping moments were computed by averaging readings over a set scan period. The moments were corrected for structural and still-air damping and reduced to aerodynamic coefficients with the following equation:

$$C_{m_q} + C_{m_{\dot{\alpha}}} = \frac{[(M_q)_a - (M_{q_t})_v]\ 2V_\infty}{q_\infty S d^2}$$

Magnus force is the force produced by a spinning model which acts normal to the plane created by the spin vector and the free-stream velocity. For the subject system this force is simply the side-force component measured by the balance.

Roll-damping moments are derived from the decaying spin rate of the model. The rate of change of rolling moment with spin rate is determined by the following equation:

$$\frac{\partial M_x}{\partial p} = M_{x_p} = \frac{I_x}{t_2 - t_1} \log_e \frac{p_1 - p_A}{p_2 - p_A}$$

Bearing friction moments were subtracted from the total moment by the following equation:

$$\left\{M_{x_p}\right\}_a = M_{x_p} - \left\{(M_{x_p})_v + (M_{x_p})_{F_A,F_N}\right\}$$

Since bearing friction is nonlinear with both spin rate and model loads, curve fits were made of $(M_{x_p})_v$ versus p and $(M_{x_p})_{F_A,F_N}$ versus F_A and F_N for on-line data reduction. Data supplied by the bearing manufacturer were used to define load effects on bearing friction. The moments were reduced to aerodynamic coefficients by the following equations:

$$C\ell_p = \frac{-2V_\infty}{q_\infty S d^2} \left\{M_{x_p}\right\}_a$$

and

$$C\ell_\delta = \frac{-p_A\, d}{2V_\infty\, \delta_F} (C\ell_p)$$

3.3 PRECISION OF MEASUREMENTS

The estimated precision of the data presented in this report, based on a 95-percent confidence level, is given below and in Fig. 4. The error sources considered for the coefficients were balance uncertainties, Mach number nonuniformities, instrument errors, and Mach number calibration accuracies.

$\Delta C\ell_p$	±0.1
$\Delta(C_{m_q} + C_{m_{\dot{\alpha}}})$	±1.5
ΔC_{n_p}	±0.1
ΔC_{Y_p}	±0.1
Δp	±0.1
$\Delta(pd/2V_\infty)$	±0.0003
$\Delta\alpha$	±0.1
$\Delta\phi$	±0.1

The uncertainties in Mach number include variation of Mach number along the tunnel centerline, instrument errors, and errors in data acquisition techniques.

SECTION IV
RESULTS AND DISCUSSION

4.1 STATIC STABILITY PHASE

The variations of C_N, C_m, and C_A with roll angle are presented in Figs. 5 and 6 for configurations $B_S N_{S2} A_{S1} F_{S2}$ and $B_S N_{S2} A_{S1} F_{S5}$ (Fig. 2a), respectively. Normal-force variations with roll angle in general were equal in magnitude to the additional lift caused by the fin incidence at the low angles of attack; however, at the higher angles the variations were larger. This was attributable to the fin-body interference effects at the higher angles of attack. These same effects were even more apparent in the pitching-moment curves. Maximum axial force occurred at approximately ϕ = 30 deg, rather than ϕ = 0 deg, which was probably due to model asymmetries or tunnel flow misalignment.

The effects of roll angle and angle of attack on C_Y, C_n, and C_ℓ are presented in Figs. 7 and 8 for configurations $B_S N_{S2} A_{S1} F_{S2}$ and $B_S N_{S2} A_{S1} F_{S5}$, respectively. Side-force and yawing-moment coefficients peaked out at approximately 45-deg roll angle. At M_∞ = 0.8, α = 20 deg on the short-fin configuration (Fig. 7d), the side-force coefficient exhibited large variations above ϕ = 60 deg. Rolling-moment coefficients exhibited two distinct peaks in the roll angle range from 0 to 180 deg. The two peaks occurred at approximately ϕ = 60 and 135 deg, and in most cases the 60-deg peak was the largest. The peaks became more pronounced as angle of attack and Mach number were increased.

The variation of pitching-moment coefficient with angle of attack for the two fin heights is presented in Fig. 9. The small-span fins produced stable trim angles that ranged from approximately -15 to -20 deg, whereas the trim angles for the larger fins ranged from -5 to -15 deg. In addition, the pitching-moment curves pass through C_m = 0 at a steeper slope for the larger fins; hence, they are more stable.

4.2 PITCH-DAMPING PHASE

The straight afterbody configuration with δ_F = 0 and h = 0.42 in. (Fig. 2b) was chosen to determine the pitch-damping characteristics at the trim angles which were measured in the static stability phase. The variation of pitch-damping coefficient with angle of attack is presented in Fig. 10. The model was dynamically stable at all test angles of attack.

4.3 ROLL DYNAMICS PHASE

The effects of fin cant (δ_F) on the roll-damping coefficient (C_{ℓ_p}) is presented in Fig. 11. Canting the fins caused a decrease in damping at the high angles of attack and a slight increase in damping at α = 0 for $M_\infty > 0.5$.

The effects of afterbody shape on roll-damping characteristics are presented in Fig. 12. The boattail base produced the largest damping at α = 0 for all Mach numbers because of the larger exposed fin area. For $\alpha > 0$, the boattail base also caused the largest damping for $M_\infty < 0.8$; however, above M_∞ = 0.8 the damping of the straight base configuration

was largest at most angles of attack. The roll-driving-moment coefficients (C_{ℓ_δ}) were higher with the boattail base, again attributable to the larger exposed fin area, at all conditions except $\alpha > 16$ deg and $M_\infty > 0.8$ (Fig. 12b). At $M_\infty = 1.2$, the autorotational spin rate dropped to zero at the high angles of attack.

It was determined that the variation of the magnus-force coefficient (C_Y) and magnus-moment coefficient (C_n) with peripheral speed ratio ($pd/2V_\infty$) was linear over the test spin rates; hence, the data presented are slopes which were derived from first order curve fits of C_Y and C_n versus $pd/2V_\infty$.

The effects of fin cant on C_{Y_p} and C_{n_p} are presented in Figs. 13. Only small fin cant effects were noted on C_{Y_p} until at $M_\infty > 0.8$. the C_{Y_p} curves diverged at the high angles of attack. The effects on C_{n_p} were most noticeable for $M_\infty \leq 0.9$ and $\alpha \leq 12$ deg where C_{n_p} was more positive for $\delta_F = 0$ (Fig. 13b).

Comparison of C_{Y_p} and C_{n_p} for the straight and boattail afterbodies are made in Fig. 14. C_{Y_p} was more negative with the straight afterbody for $M_\infty < 0.8$ and $\alpha > 12$ deg. Only small differences were noted at other test conditions. For both afterbodies C_{n_p} tended to large negative values as angle of attack was increased above 16 deg, with significant differences for the straight and boattail afterbodies (Fig. 14b).

SECTION V
SUMMARY OF RESULTS

The results of this investigation are summarized as follows:

1. Static Stability Phase

   a. Stable trim angles were achieved with the configurations tested.

   b. The magnitude of the trim angle decreased and the bomblet became more stable with increasing fin height.

   c. Normal-force and pitching-moment variations with roll angle were largest at the higher angles of attack.

   d. Maximum side force and yawing moment occurred at approximately 45-deg roll angle for all angles of attack.

   e. The rolling moment exhibited two peaks in the roll angle range from 0 to 180 deg.

2. Pitch-Damping Phase

   The model was dynamically stable at all test angles of attack.

3. Roll Dynamics Phase

a. Fin cant caused a decrease in roll damping except at zero angle of attack and Mach numbers greater than 0.5.

b. The boattail afterbody configuration had the largest roll damping at zero angle of attack and the largest roll-driving moment.

c. Zero autorotational spin rate was obtained at a Mach number of 1.2 at the high angles of attack.

d. The variations of magnus force and moment were linear with peripheral speed ratio.

e. Fin cant affected the magnus-force derivative at Mach numbers above 0.8 at high angles of attack only, and affected the magnus-moment derivative at Mach numbers less than 0.9 and angles of attack less than 12 deg.

f. Changing to a boattail base affected the magnus-force derivative at Mach numbers less than 0.8 and angles of attack above 12 deg. The magnus-moment derivatives were affected at high angles of attack only.

REFERENCES

1. Shadow, T. O. "Wind Tunnel Investigation of the Transonic Static Stability Characteristics of Three Bomblet Munition Models Used in the Evaluation of Aerodynamic Dispersion Techniques." AEDC-TR-70-233 (AD875110L), September 1970.

2. Shadow, T. O. "Transonic Roll-Damping and Magnus Characteristics of Three Bomblet Munition Models Used in the Evaluation of Aerodynamic Dispersion Techniques." AEDC-TR-71-33 (AD880981L), March 1971.

3. Uselton, Bob, Carman, Jack, and Shadow, Tom. "Dynamic Stability Characteristics of Axisymmetric Bomblet Munition Models at Mach Numbers 0.3 to 1.2." AEDC-TR-70-270 (AD884281L), December 1970.

4. Carman, J. B., Uselton, B. L., and Burt, G. E. "Roll-Damping, Static Stability, and Damping-in-Pitch Characteristics of Axisymmetric Bomblet Munition Models at Supersonic Mach Numbers." AEDC-TR-71-88 (AD882636L), April 1971.

5. Brunk, James E. "Aerodynamic Dispersion Techniques." AFATL-TR-70-123, November 1970.

6. Shadow, T. O. "Transonic Static Stability Characteristics of Bomblet Munition Models Used in the Evaluation of the Zero-Coning Aerodynamic Dispersal Technique." AEDC-TR-71-247 and AFATL-TR-71-144 (AD889187L), November 1971.

7. Test Facilities Handbook (Ninth Edition). "Propulsion Wind Tunnel Facility, Vol. 4." Arnold Engineering Development Center, July 1971.

8. Welsh, C. J., Hance, Q. P., and Ward, L. K. "A Forced-Oscillation Balance System for the von Kármán Gas Dynamics Facility 40-by 40-Inch Supersonic Tunnel." AEDC-TN-61-63 (AD257380), May 1961.

APPENDIXES

I. ILLUSTRATIONS
II. TABLES

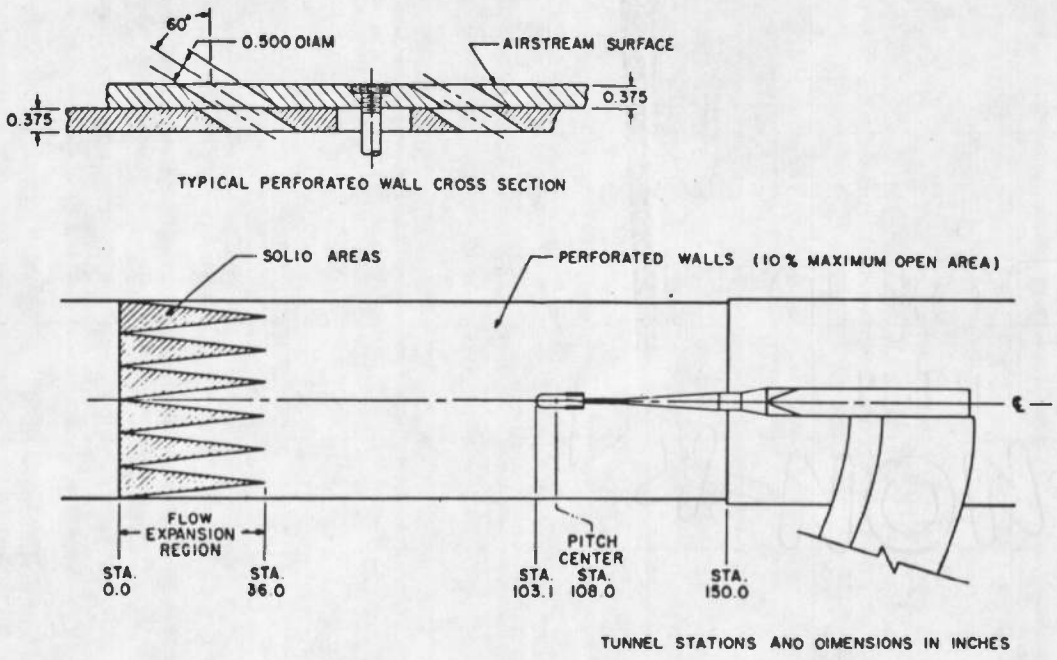

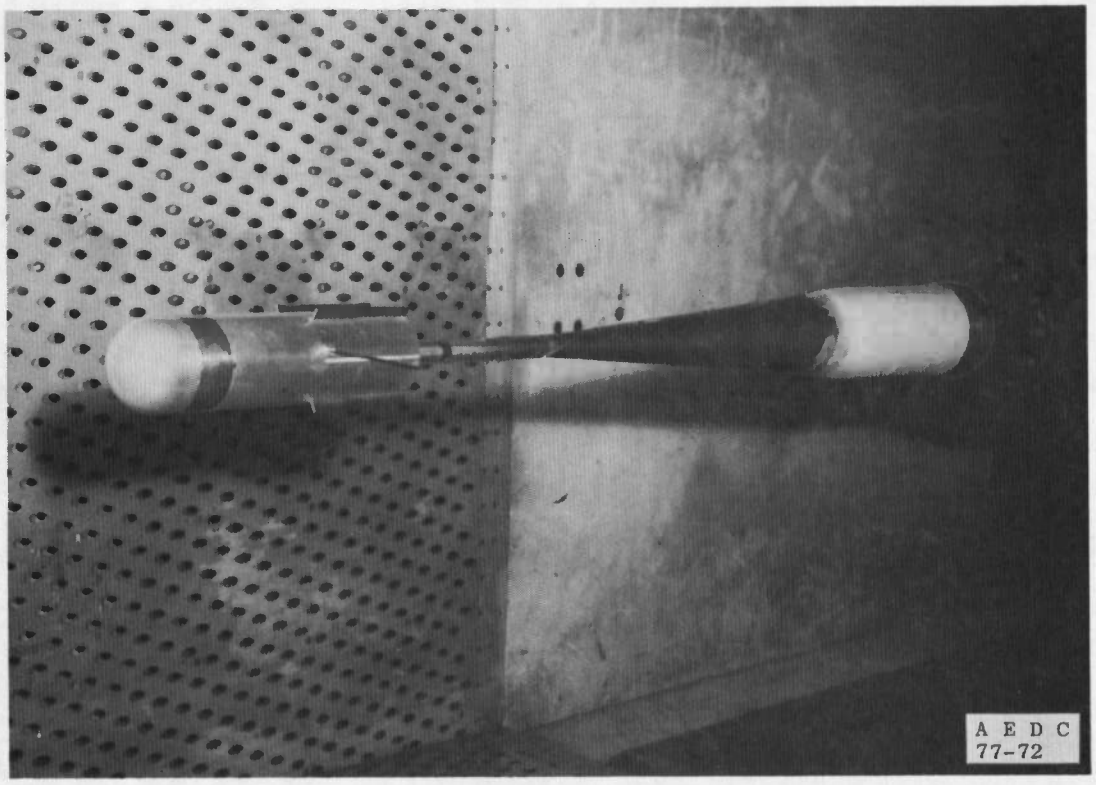

a. Static Stability Phase

Fig. 1 Schematics and Photographs of Test Installations

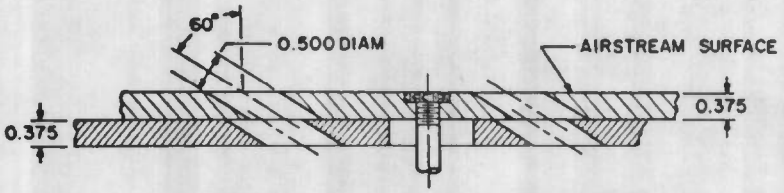

TYPICAL PERFORATED WALL CROSS SECTION

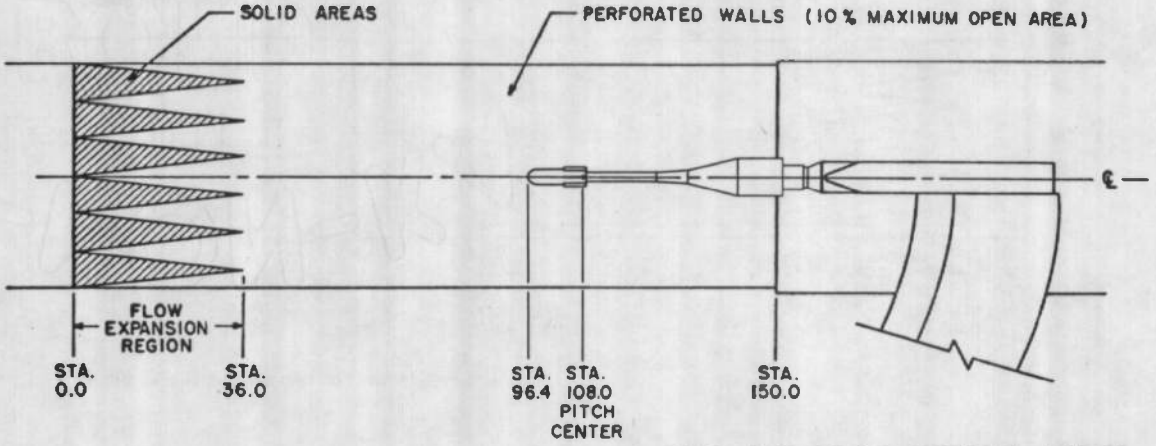

TUNNEL STATIONS AND DIMENSIONS IN INCHES

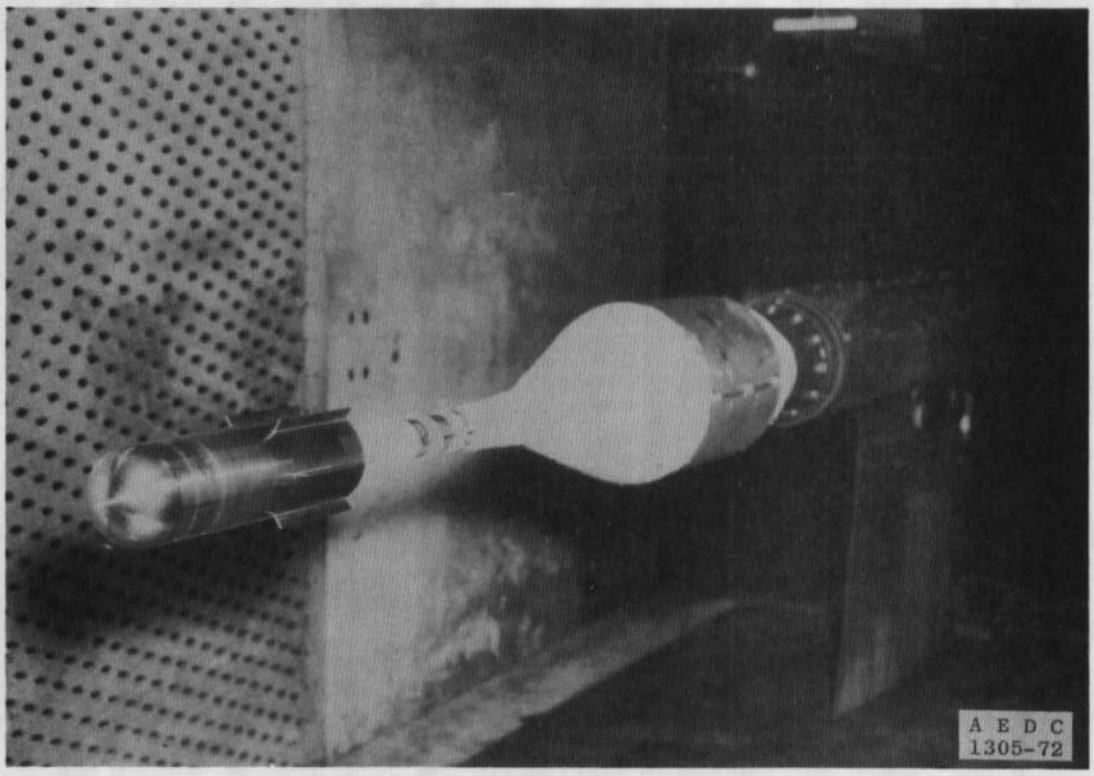

b. Pitch-Damping Base

Fig. 1 Continued

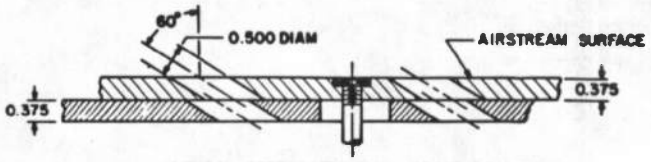

TYPICAL PERFORATED WALL CROSS SECTION

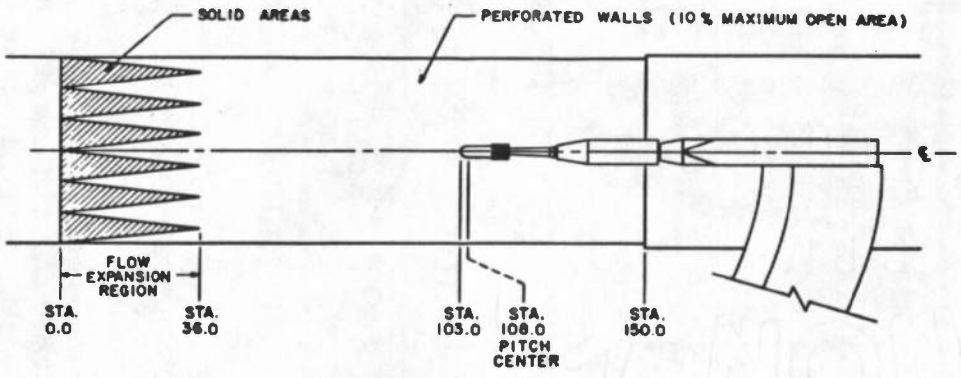

TUNNEL STATIONS AND DIMENSIONS IN INCHES

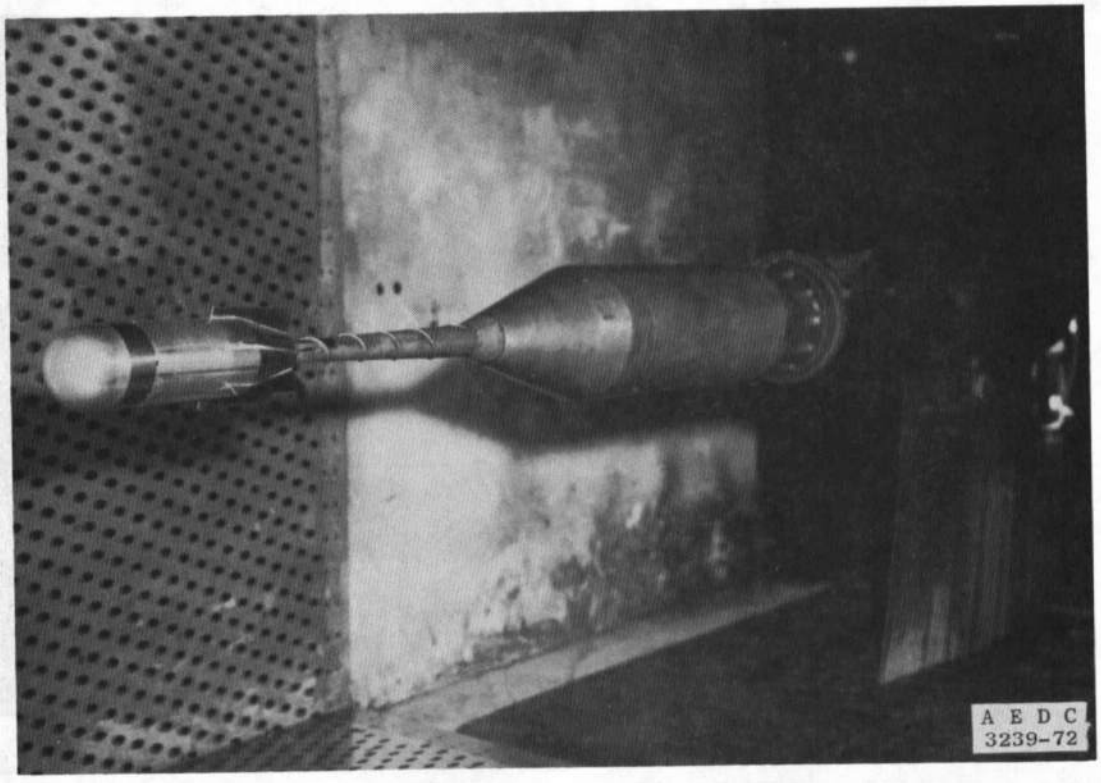

c. Roll Dynamics Phase
Fig. 1 Concluded

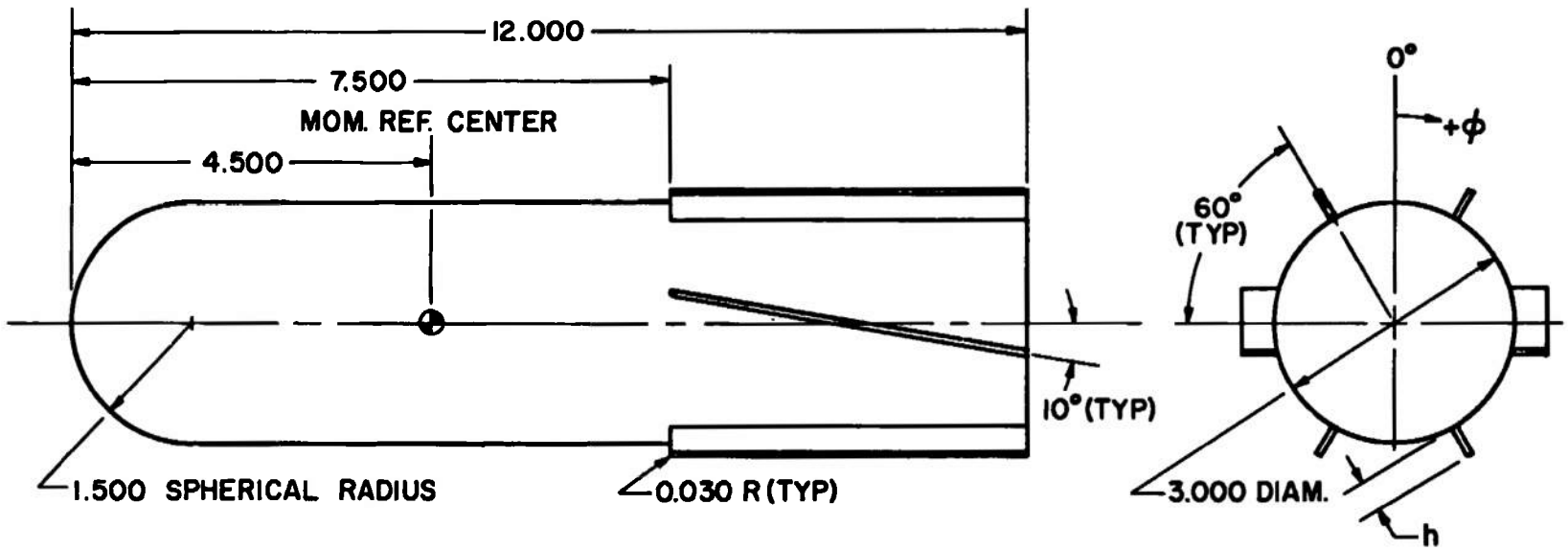

CONFIGURATION	h
$B_S N_{S2} A_{S1} F_{S2}$	0.233
$B_S N_{S2} A_{S1} F_{S5}$	0.420

ALL DIMENSIONS IN INCHES

a. Static Stability Phase

Fig. 2 Details and Dimensions of Test Articles

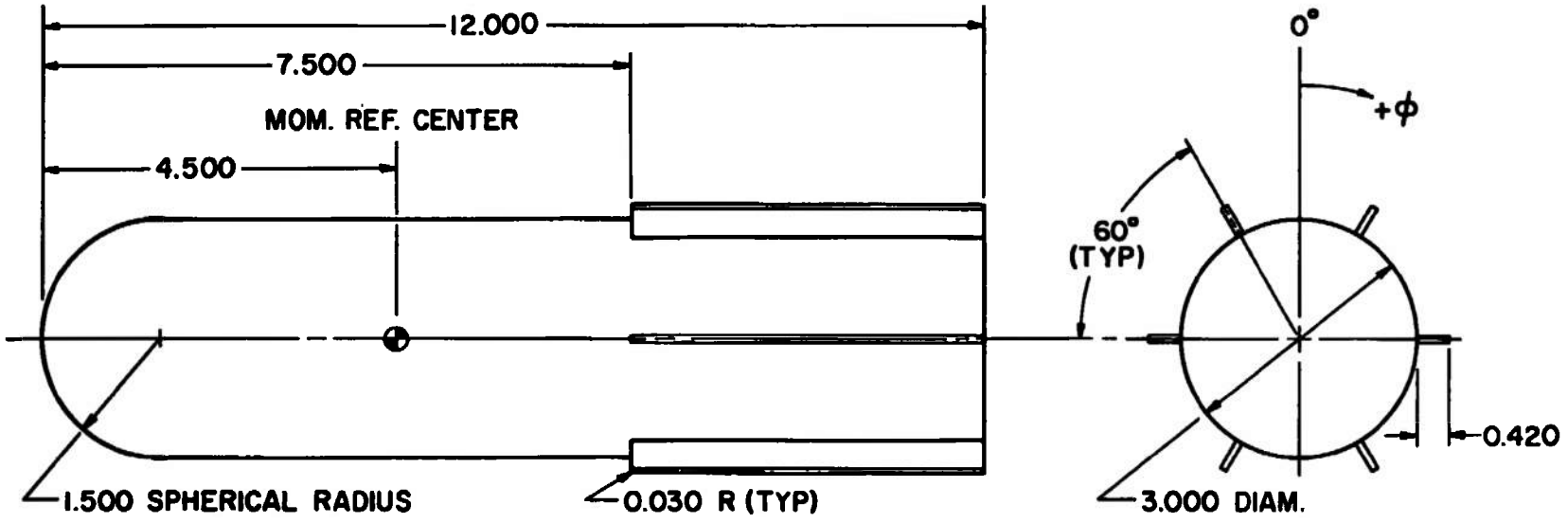

CONFIGURATION $B_S N_{S2} A_{S1} F_{S5}$

ALL DIMENSIONS IN INCHES

b. Pitch-Damping Phase
Fig. 2 Continued

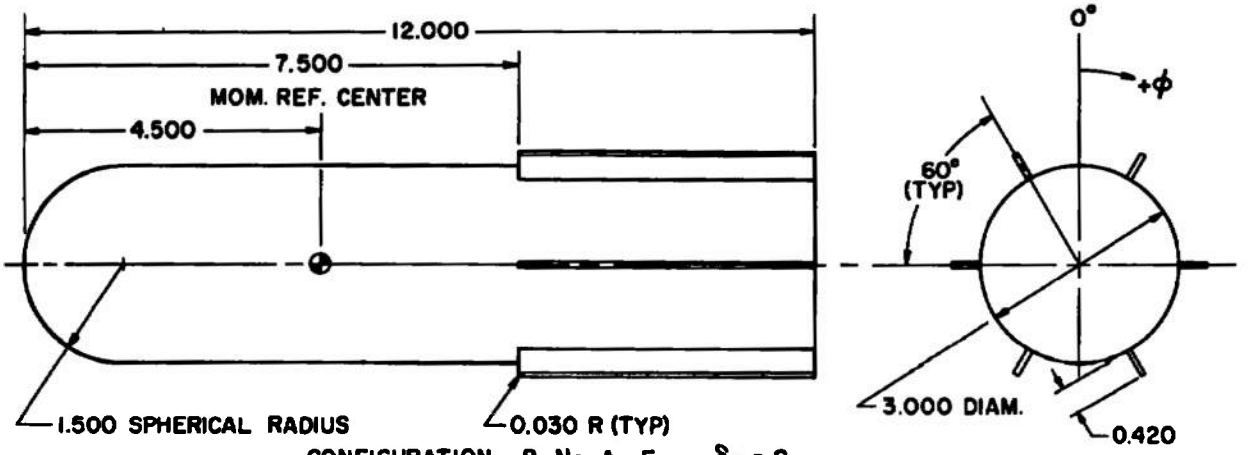

CONFIGURATION $B_S N_{S2} A_{S1} F_{S5}$, $\delta_F = 0$

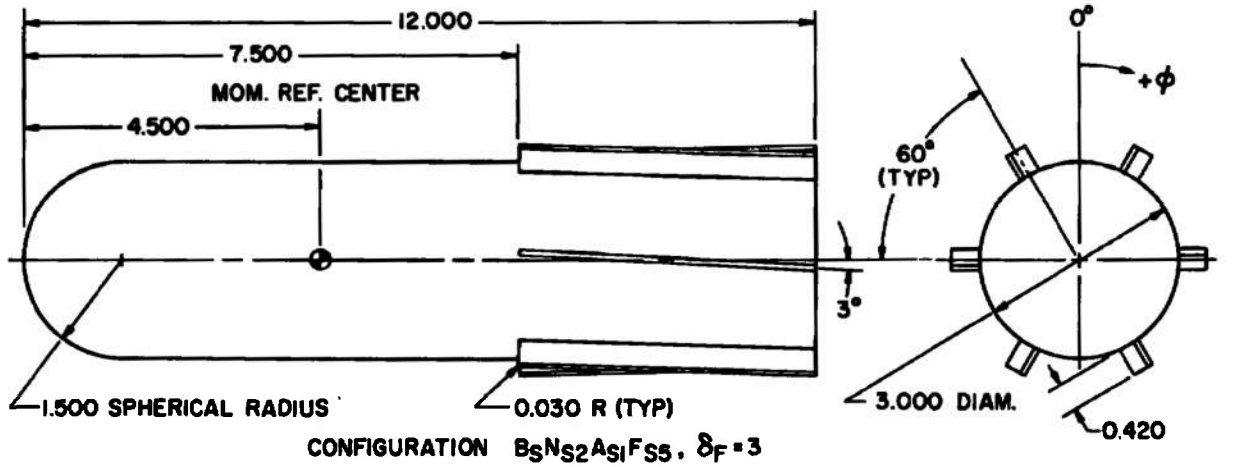

CONFIGURATION $B_S N_{S2} A_{S1} F_{S5}$, $\delta_F = 3$

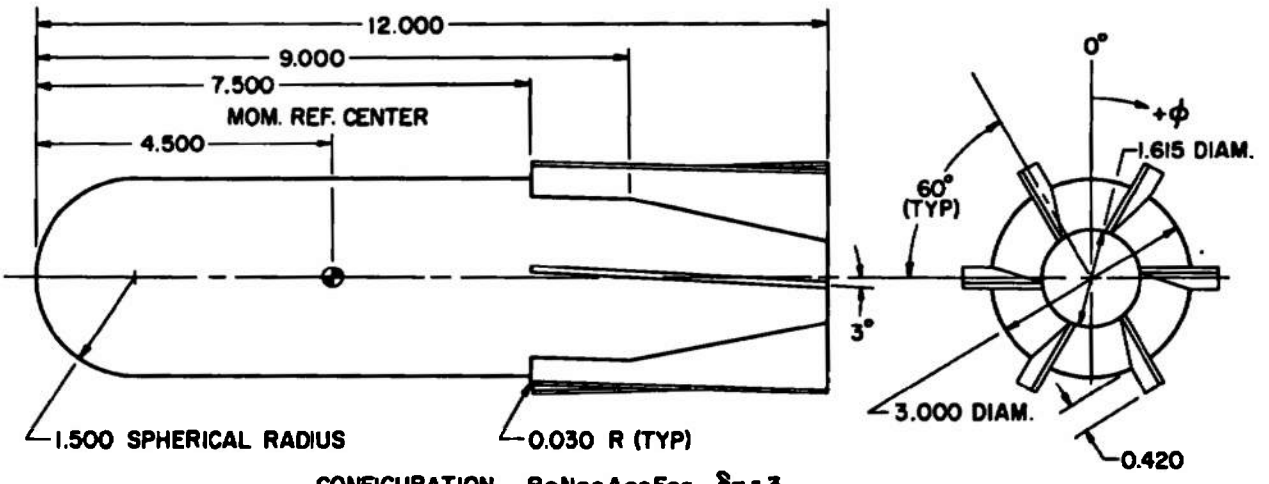

CONFIGURATION $B_S N_{S2} A_{S2} F_{S5}$, $\delta_F = 3$

ALL DIMENSIONS IN INCHES

c. Roll Dynamics Phase

Fig. 2 Concluded

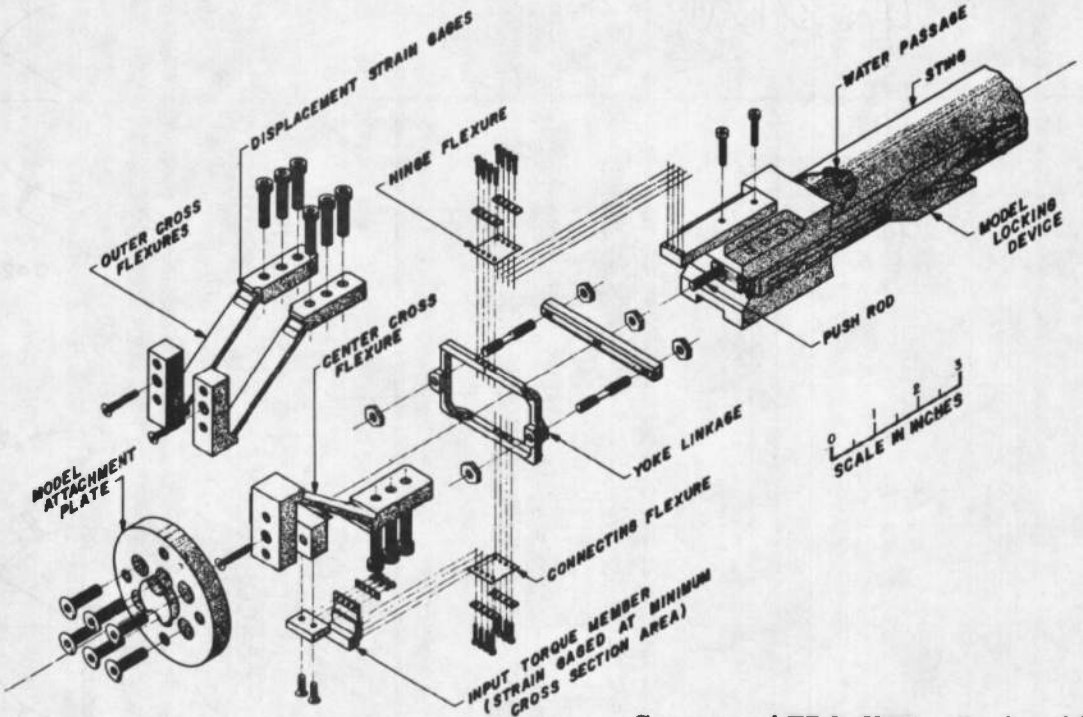

Source AEDC-VKF, Ref. 56

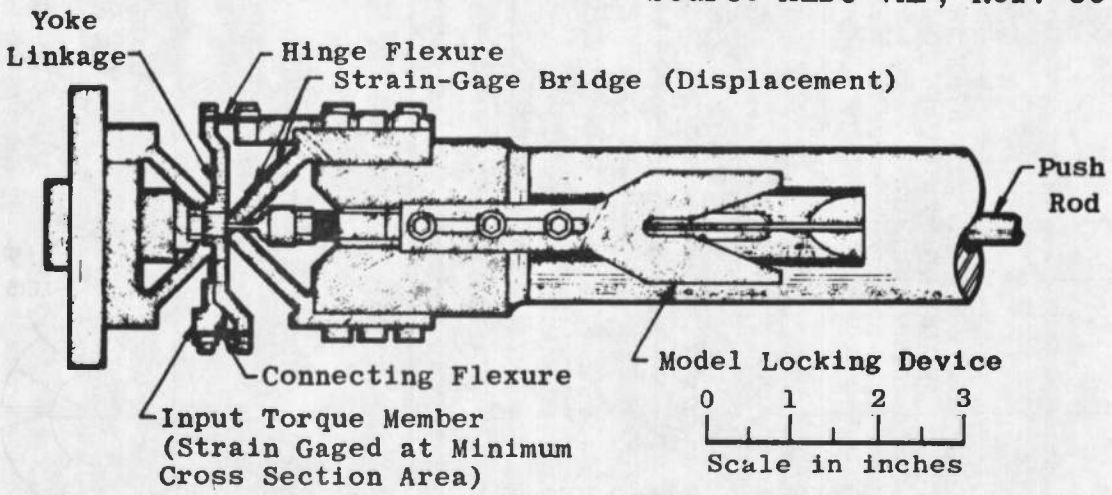

a. Pitch Damping

Fig. 3 Pitch-Damping and Roll Dynamics Test Mechanisms

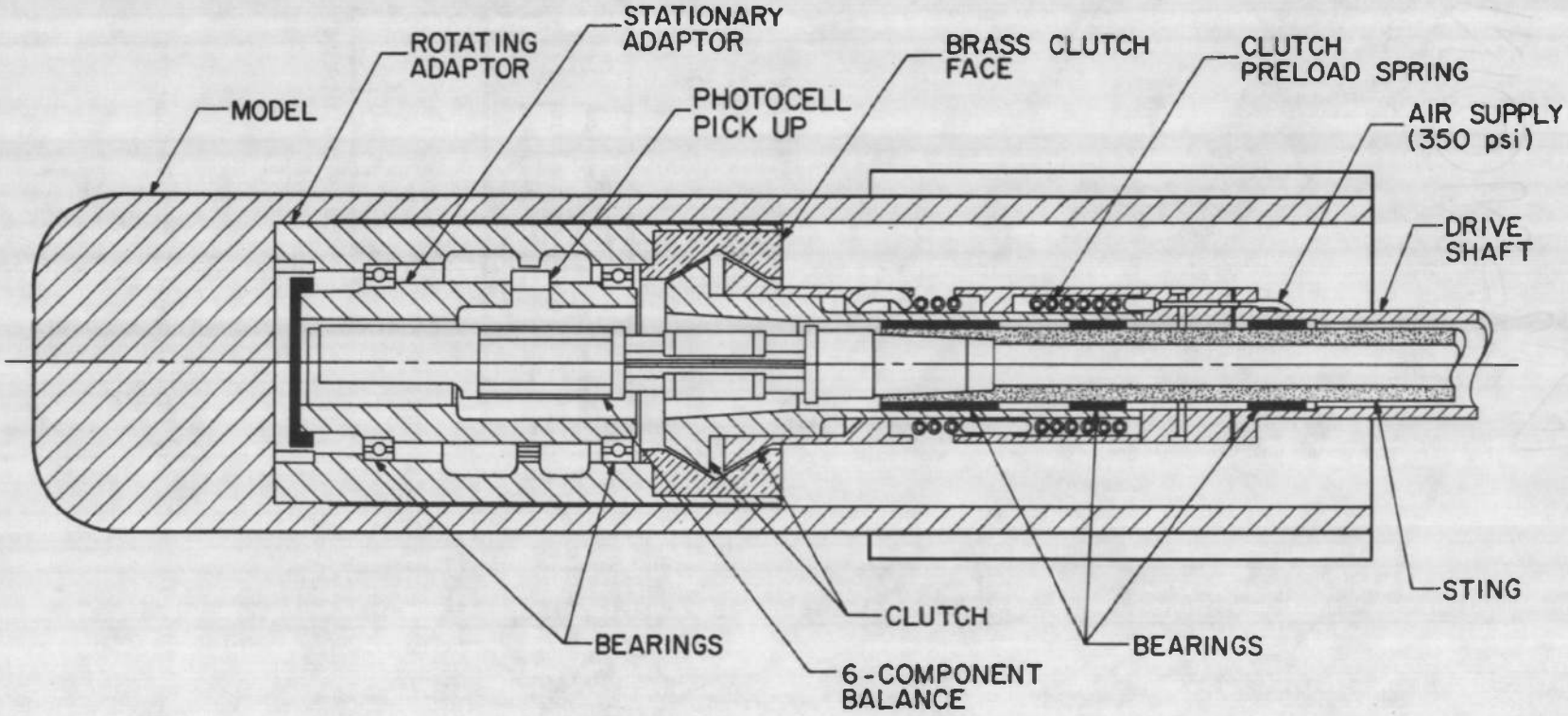

b. Roll Dynamics
Fig. 3 Concluded

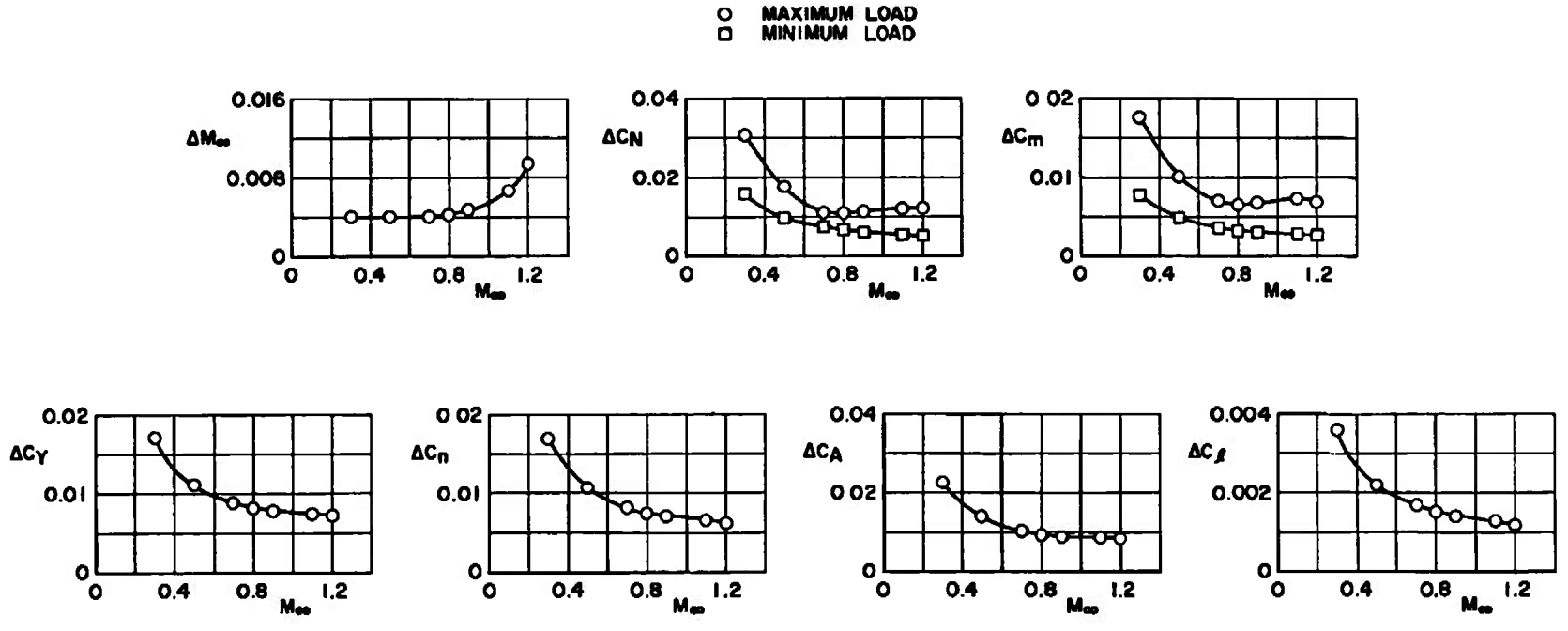

Fig. 4 Estimated Precision of Data

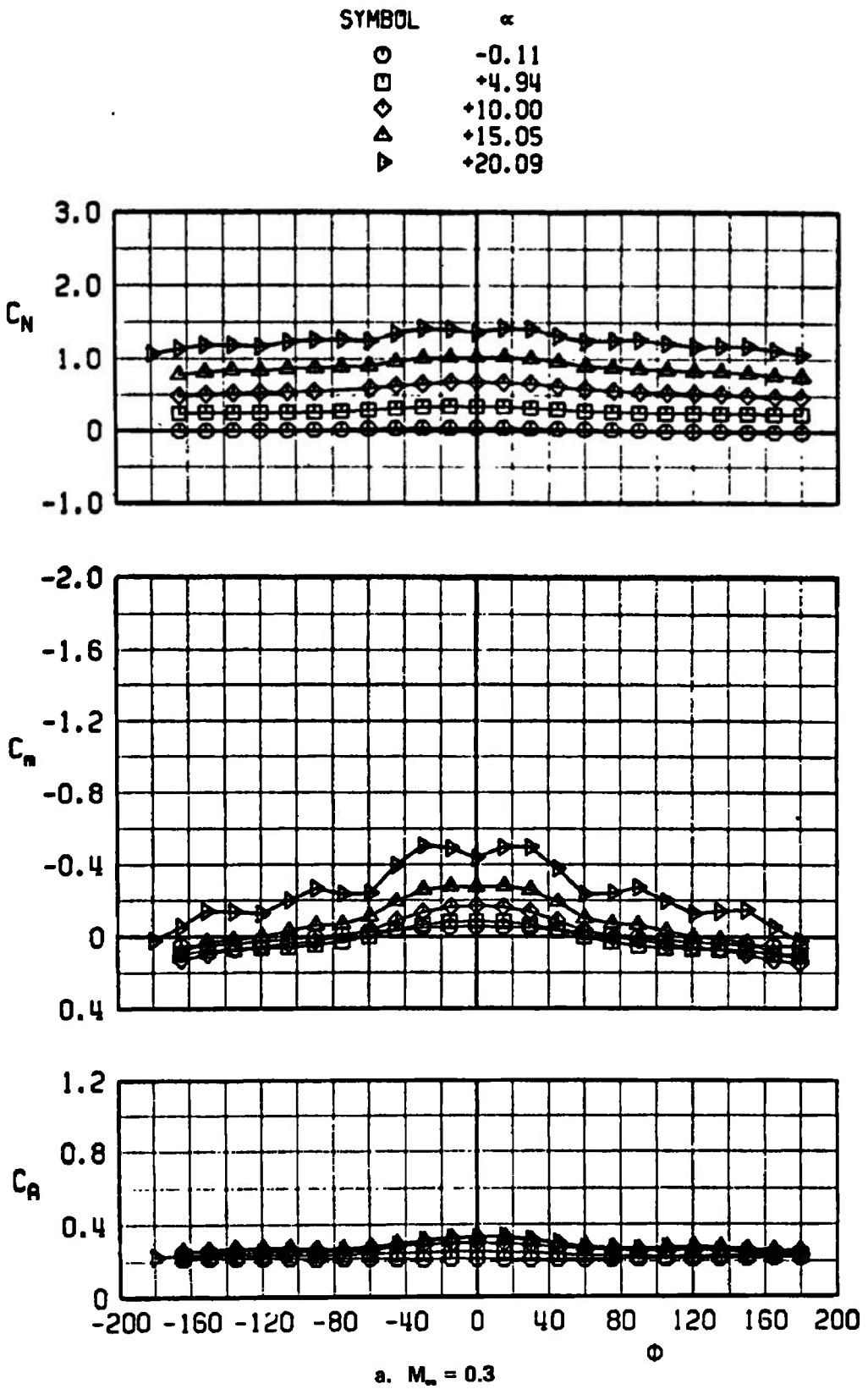

a. $M_\infty = 0.3$

Fig. 5 Variation of C_N, C_m, and C_A with Roll Angle for Configuration $B_S N_{S2} A_{S1} F_{S2}$

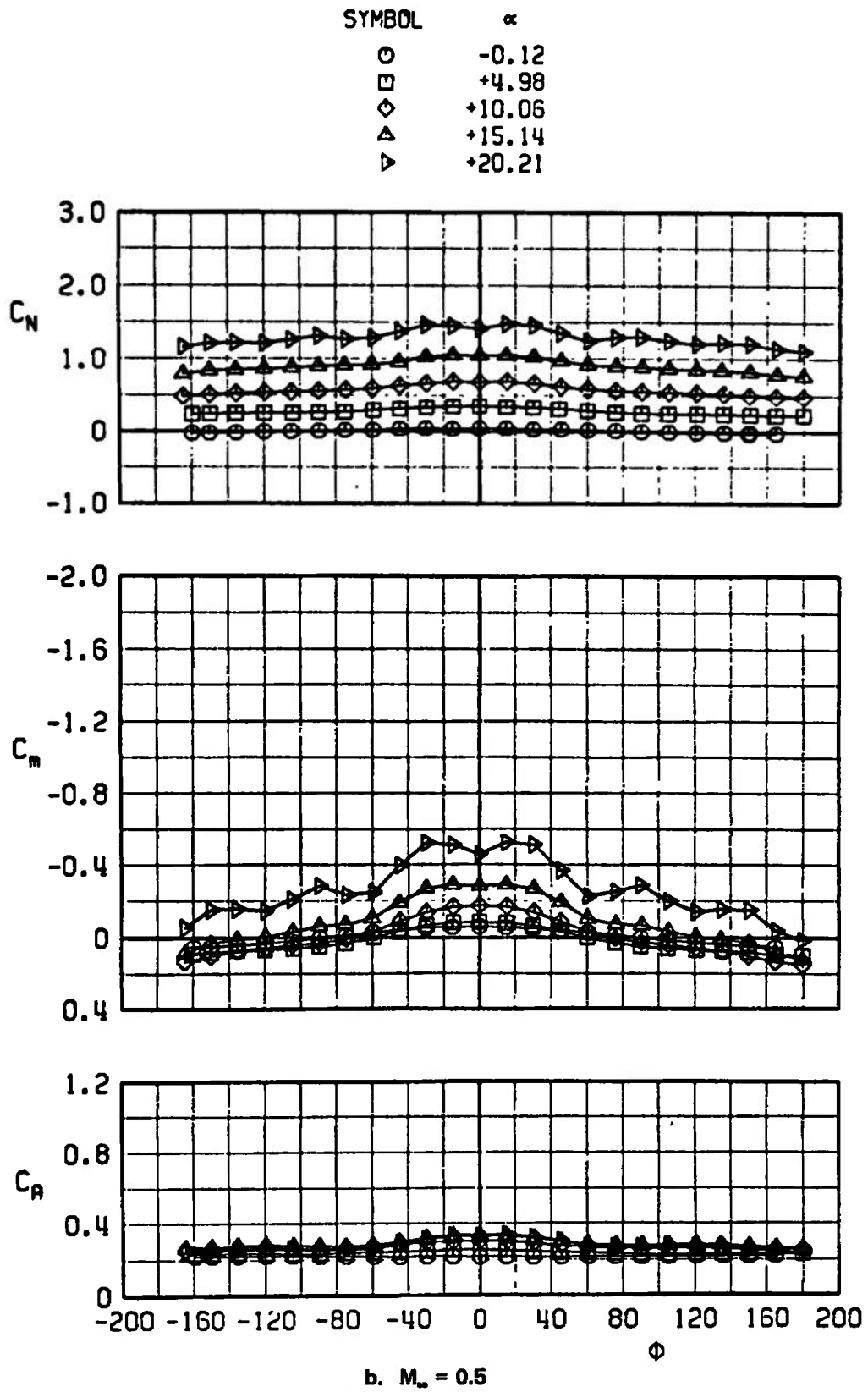

b. $M_\infty = 0.5$

Fig. 5 Continued

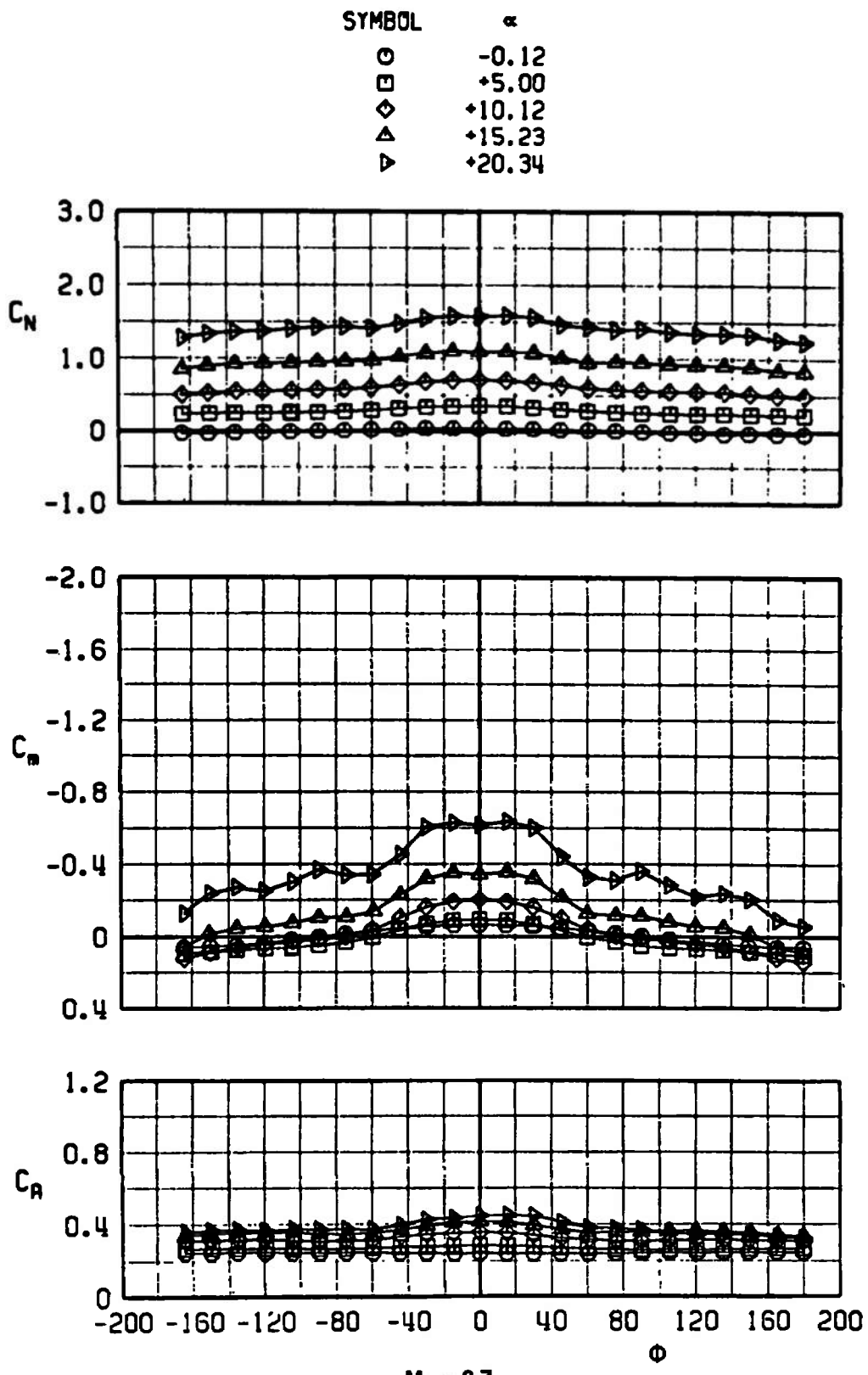

c. $M_\infty = 0.7$

Fig. 5 Continued

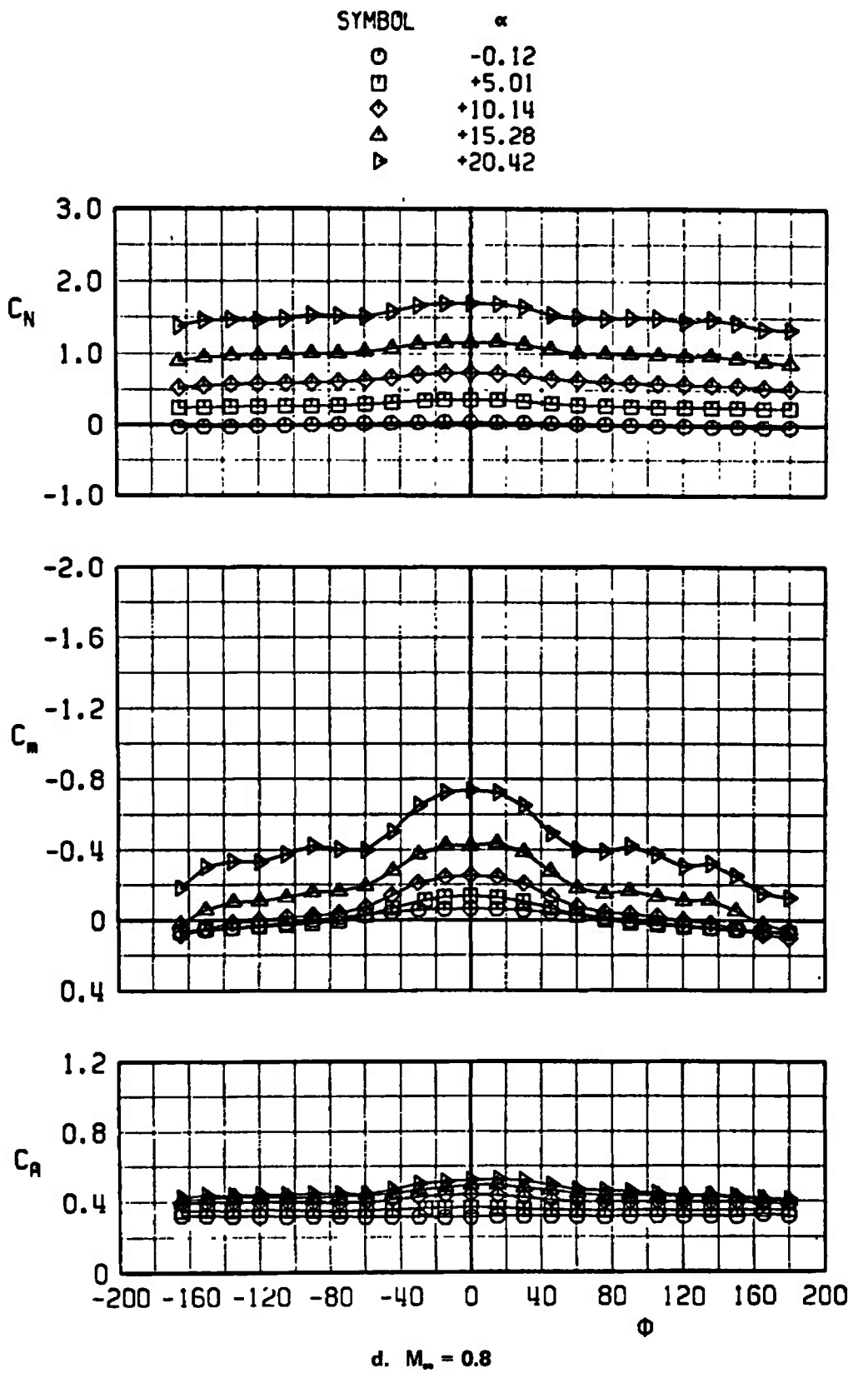

d. $M_\infty = 0.8$

Fig. 5 Continued

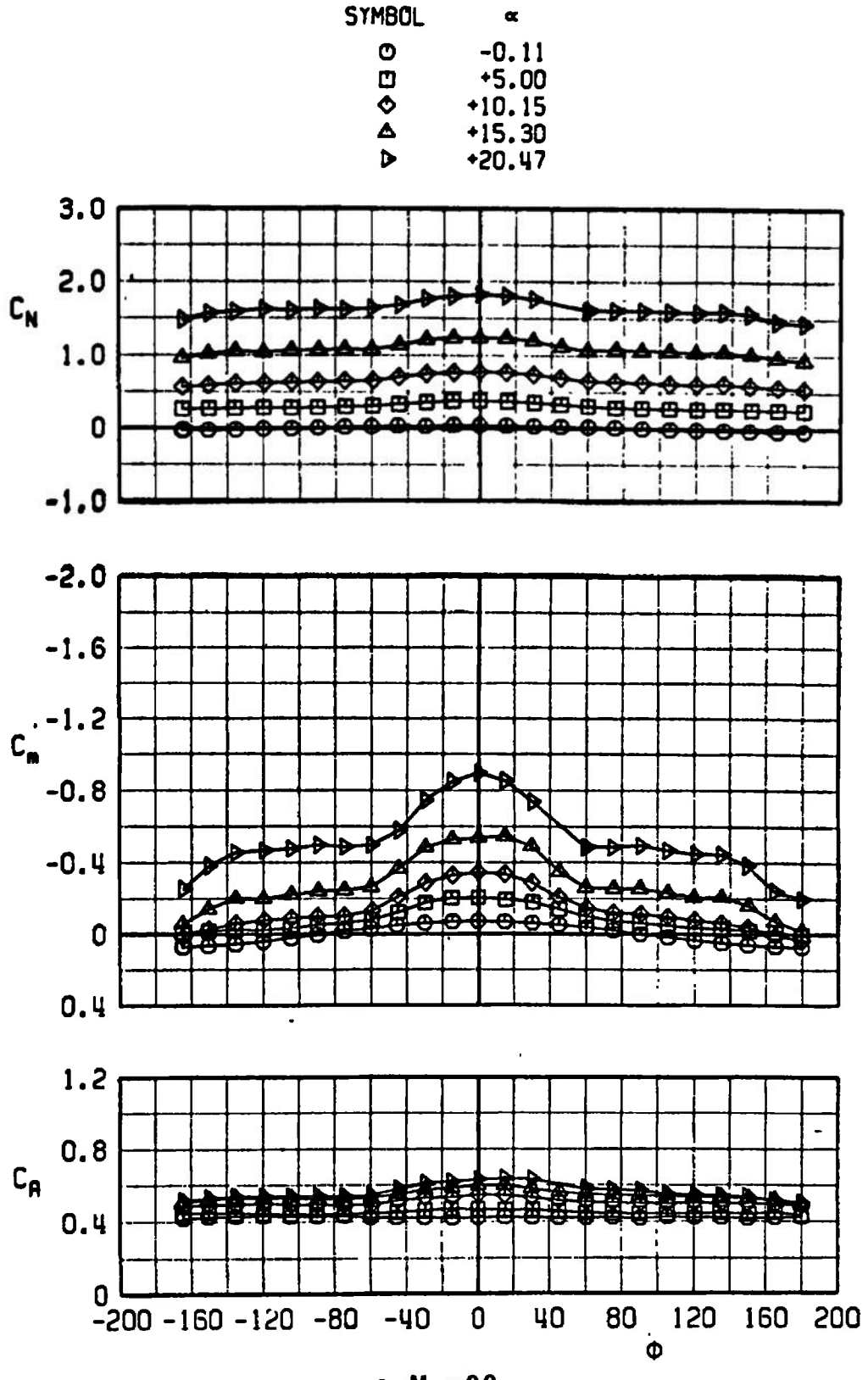

e. $M_\infty = 0.9$

Fig. 5 Continued

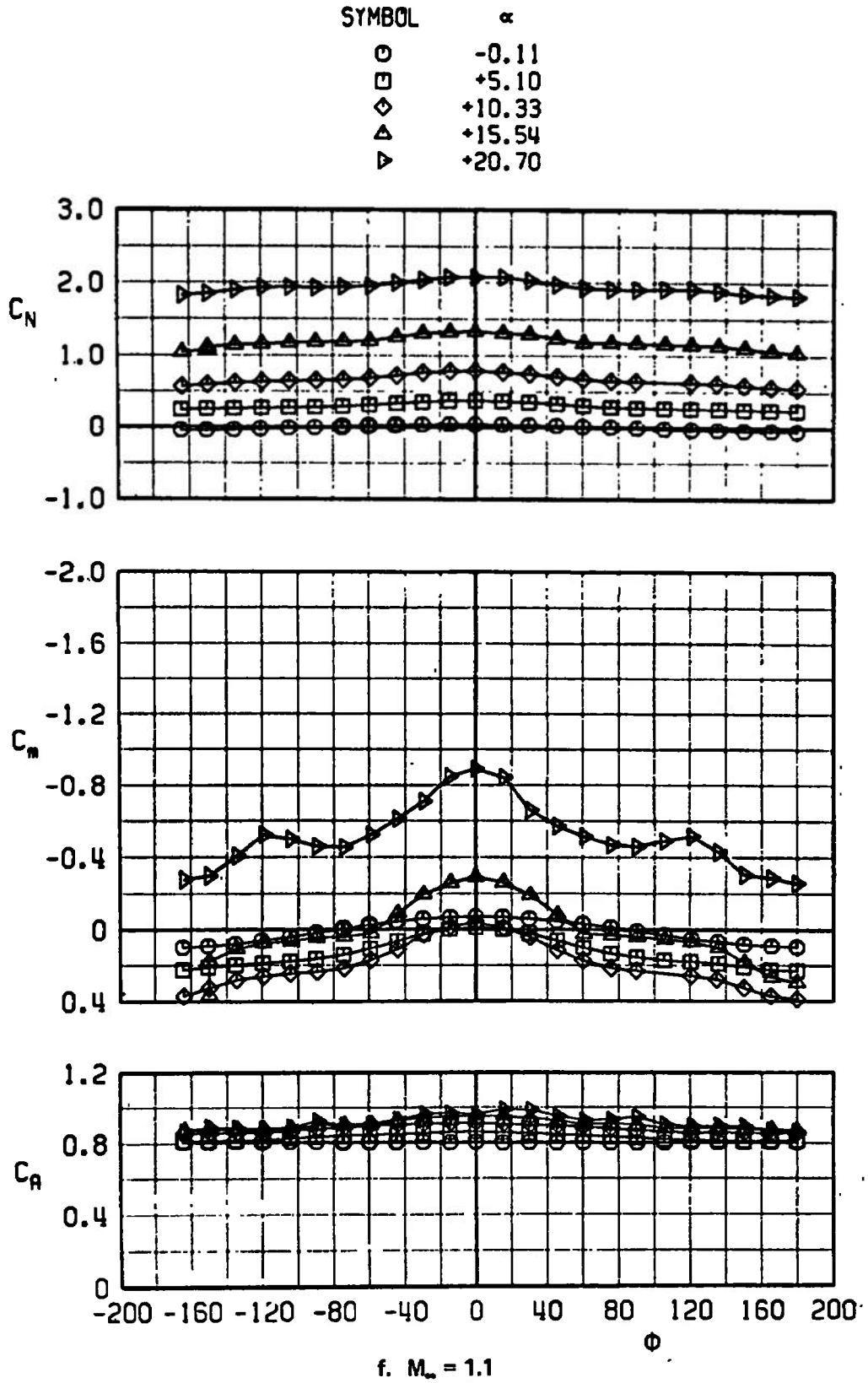

f. $M_\infty = 1.1$

Fig. 5 Continued

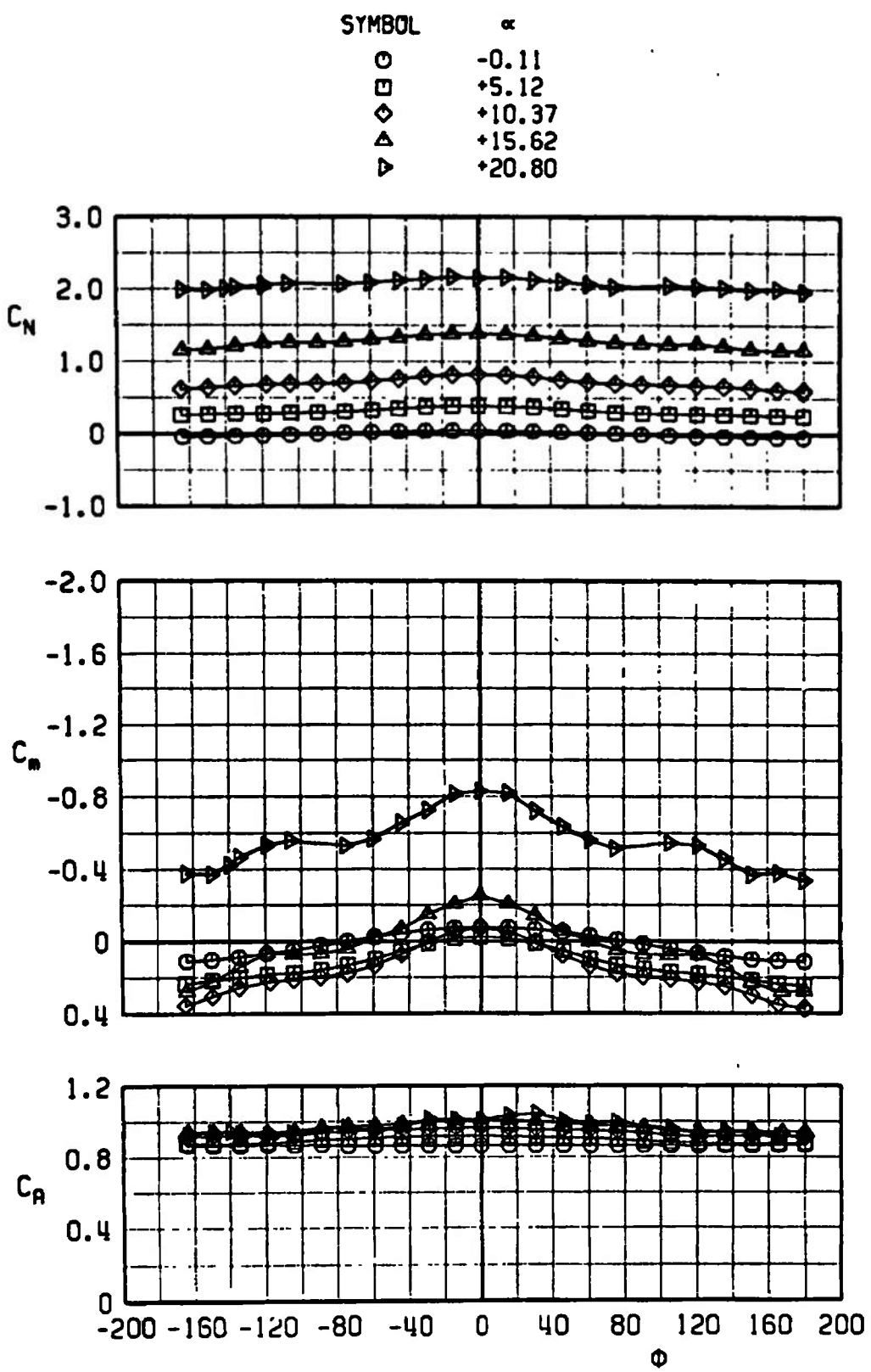

g. $M_\infty = 1.2$

Fig. 5 Concluded

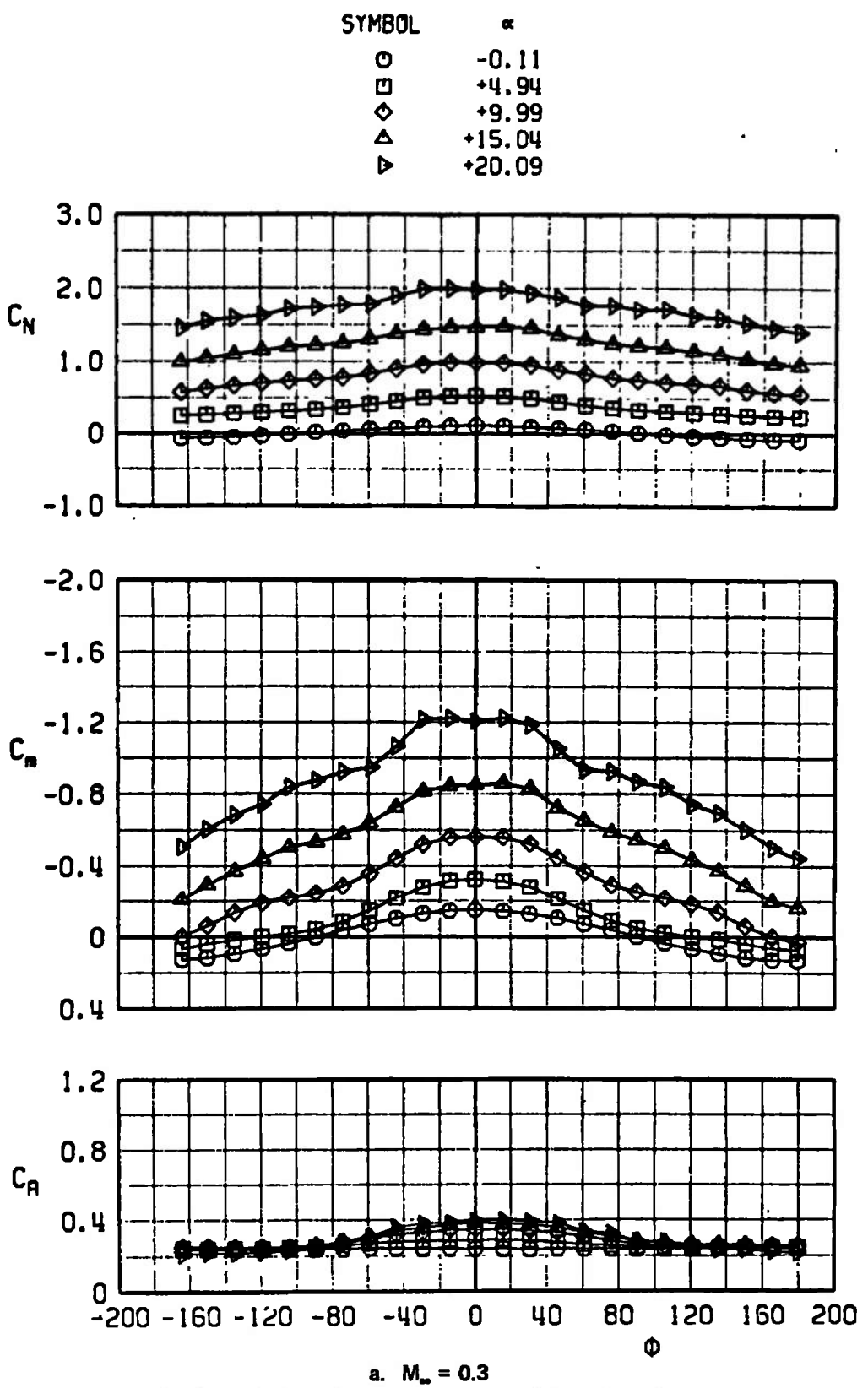

a. $M_\infty = 0.3$

Fig. 6 Variation of C_N, C_m, and C_A with Roll Angle for Configuration $B_S N_{S2} A_{S1} F_{S5}$

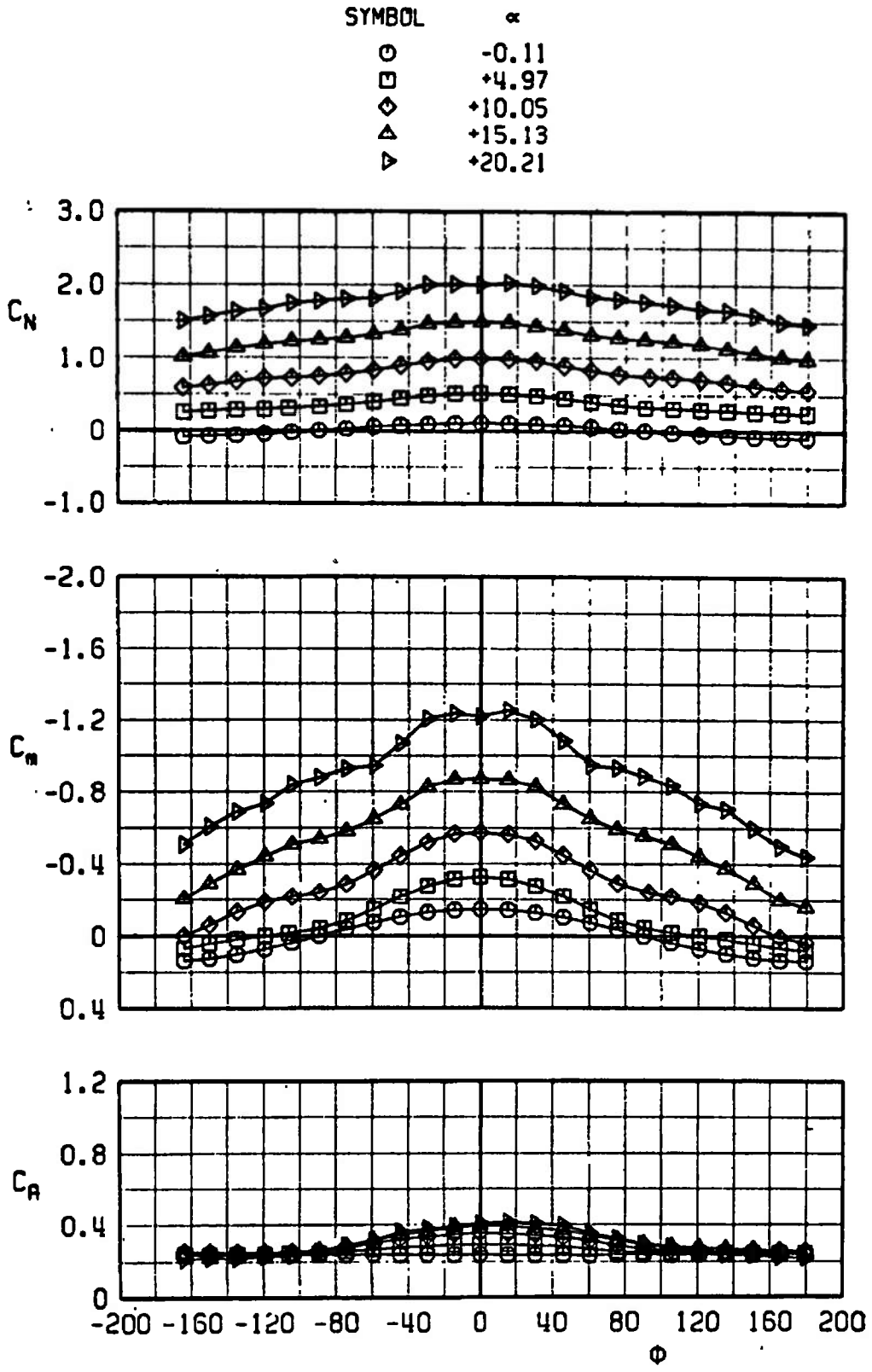

b. $M_\infty = 0.5$

Fig. 6 Continued

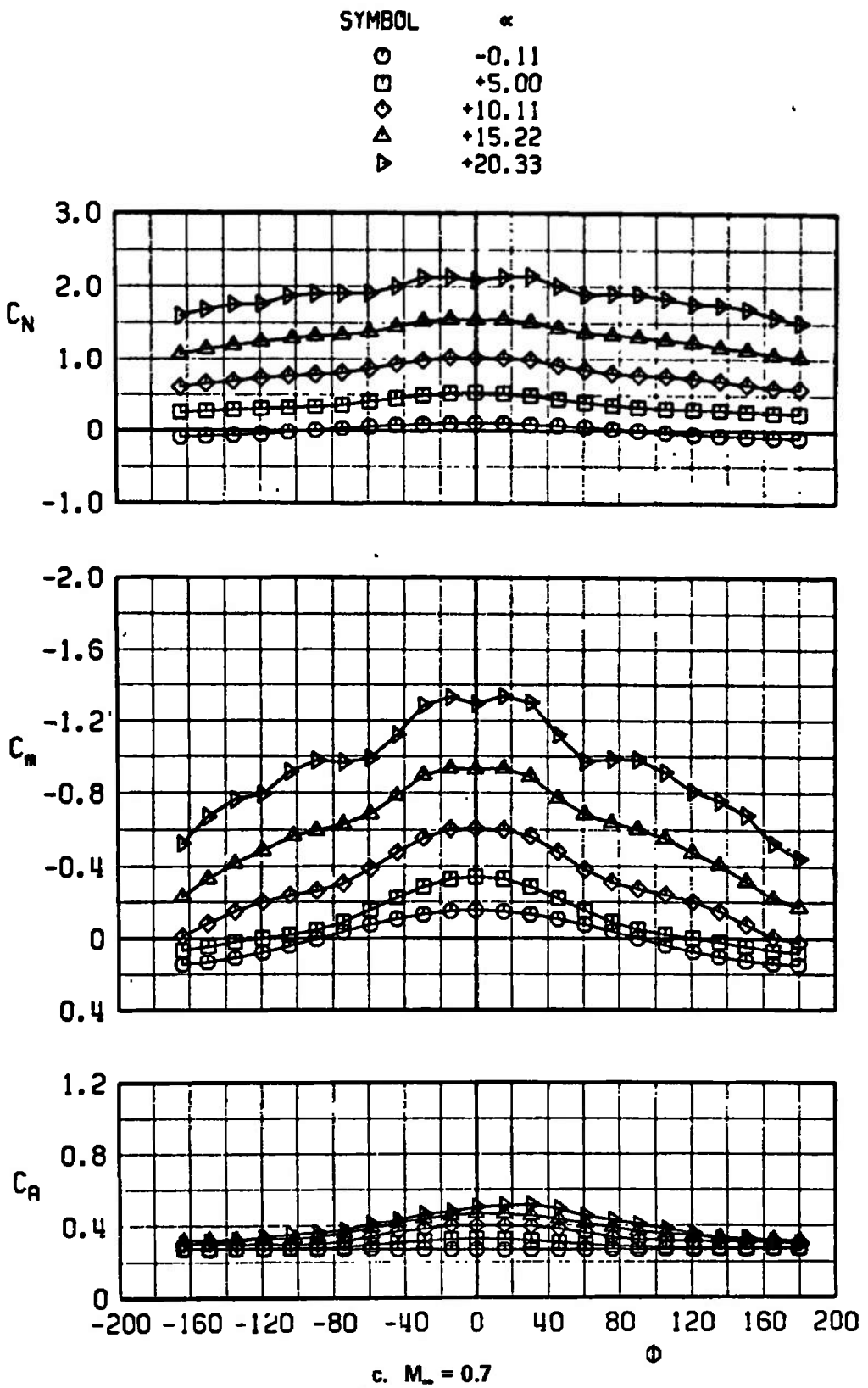

c. $M_\infty = 0.7$

Fig. 6 Continued

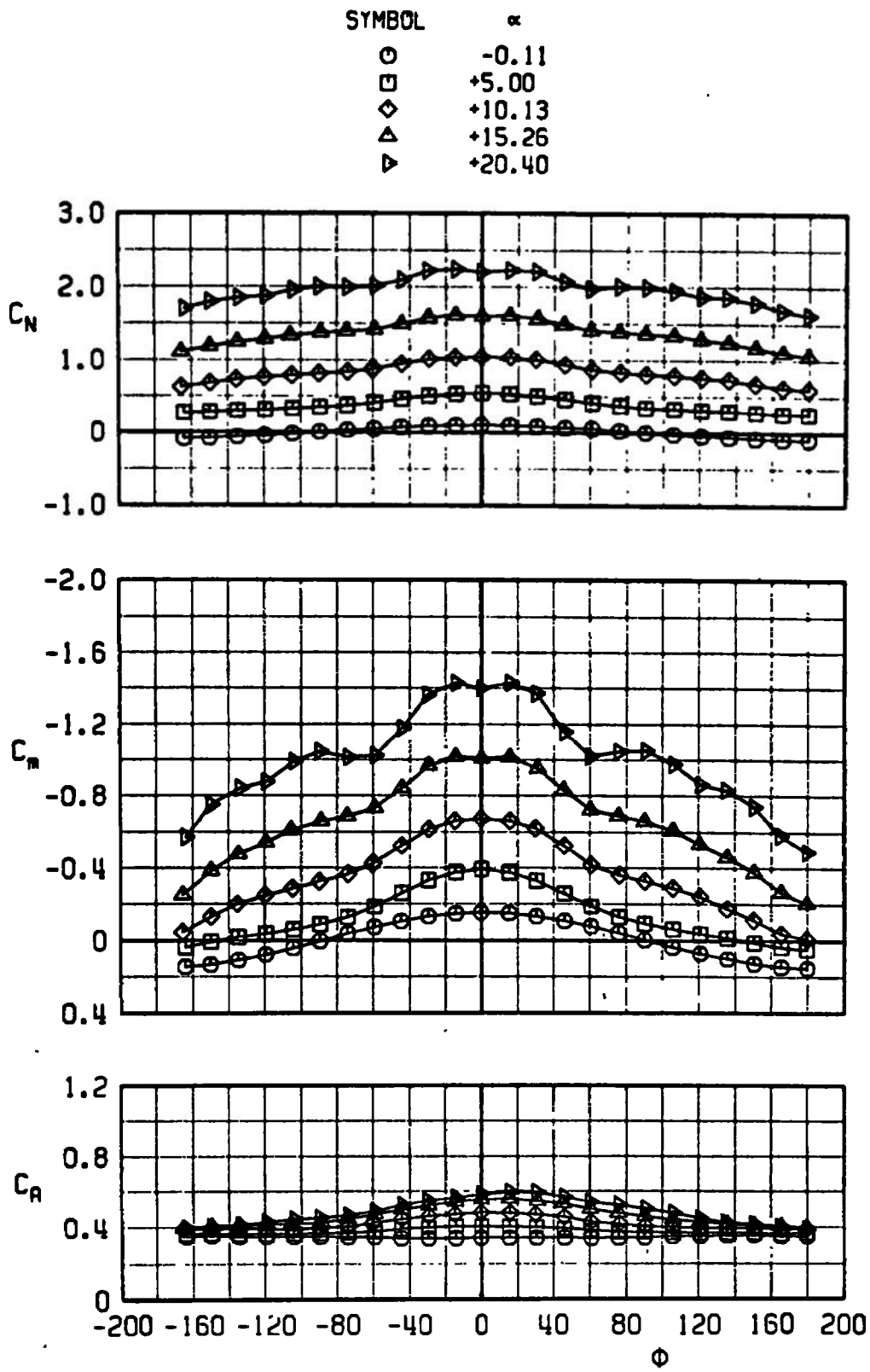

d. $M_\infty = 0.8$

Fig. 6 Continued

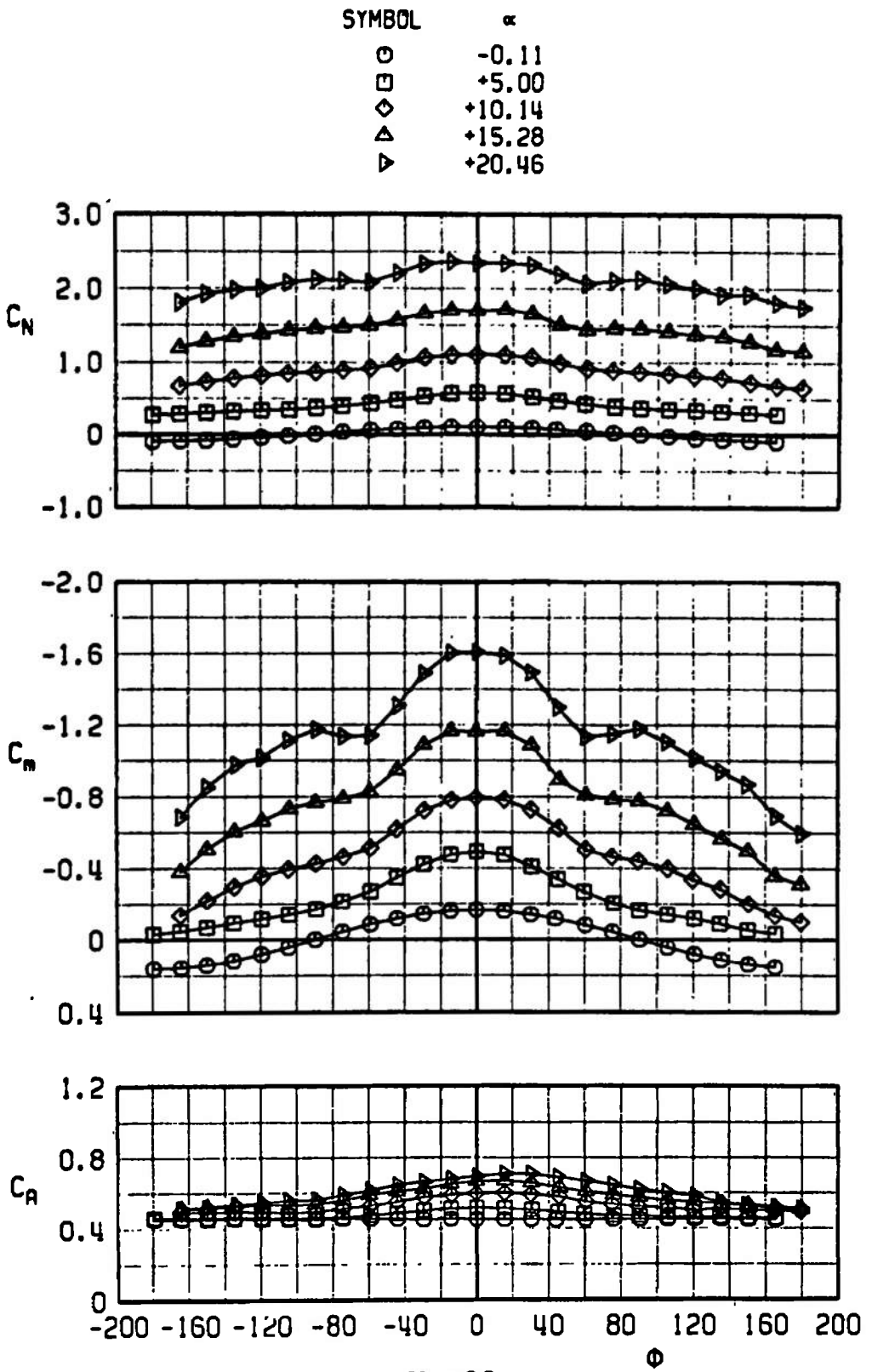

e. $M_\infty = 0.9$

Fig. 6 Continued

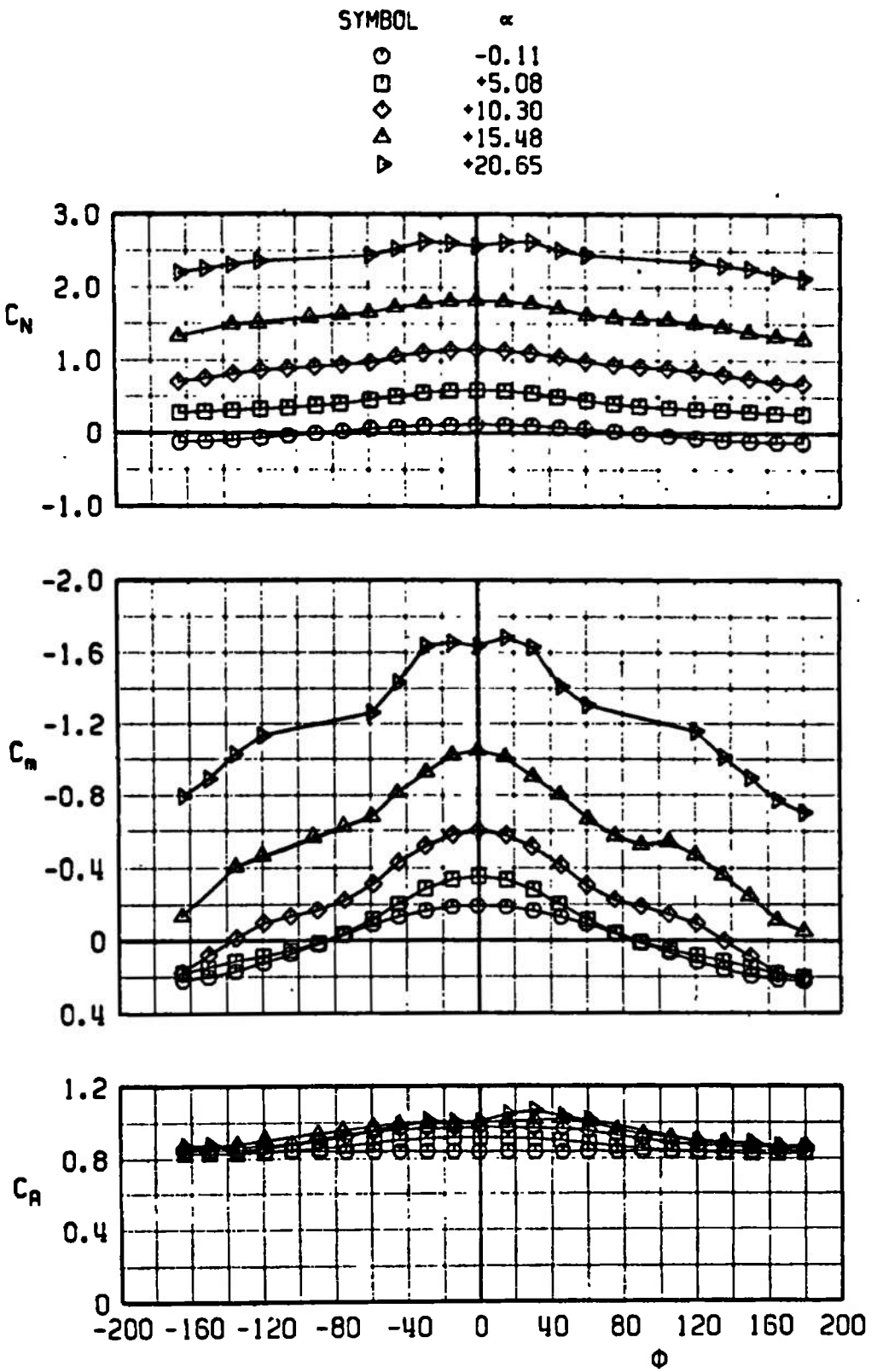

f. $M_\infty = 1.1$

Fig. 6 Continued

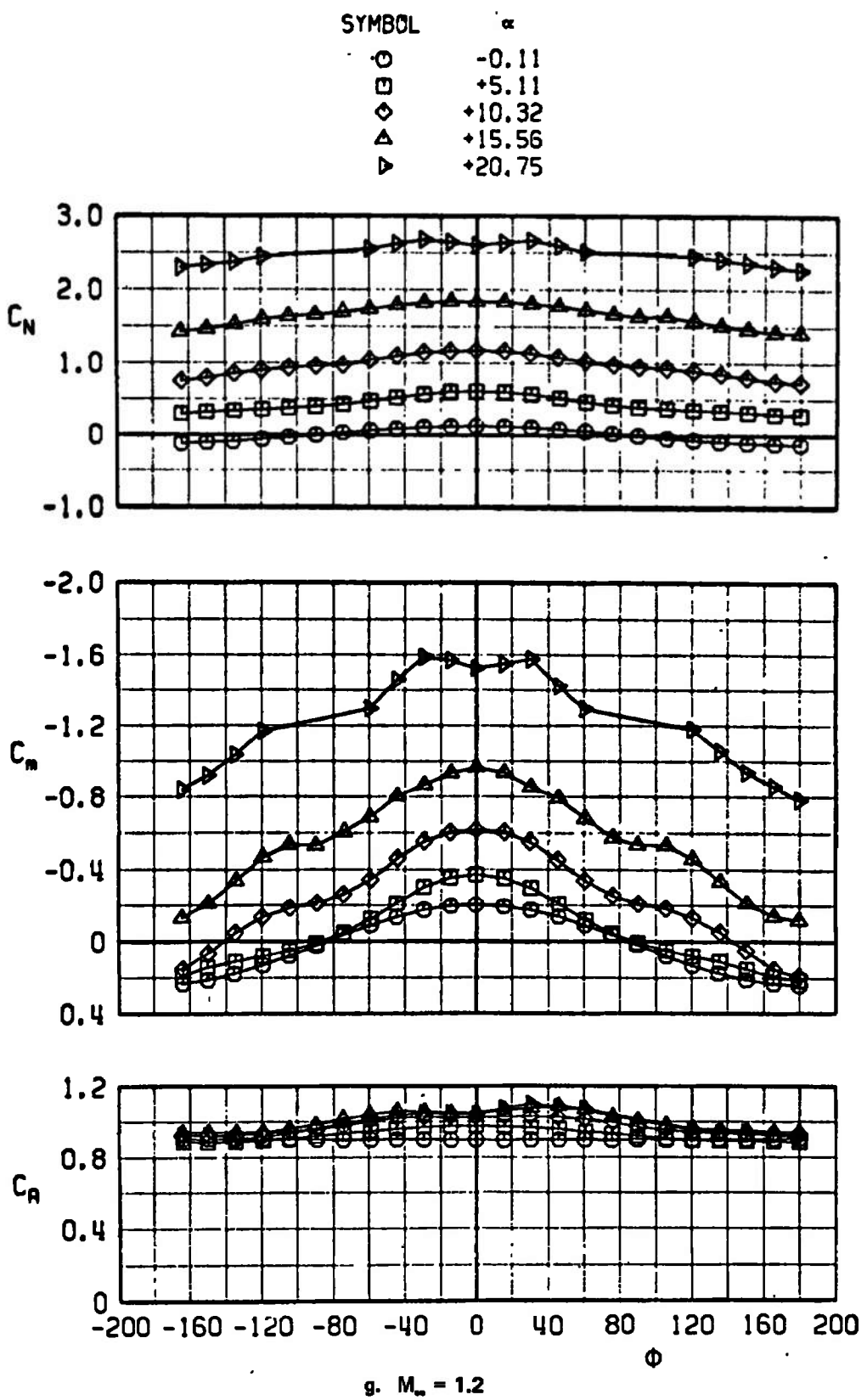

g. $M_\infty = 1.2$

Fig. 6 Concluded

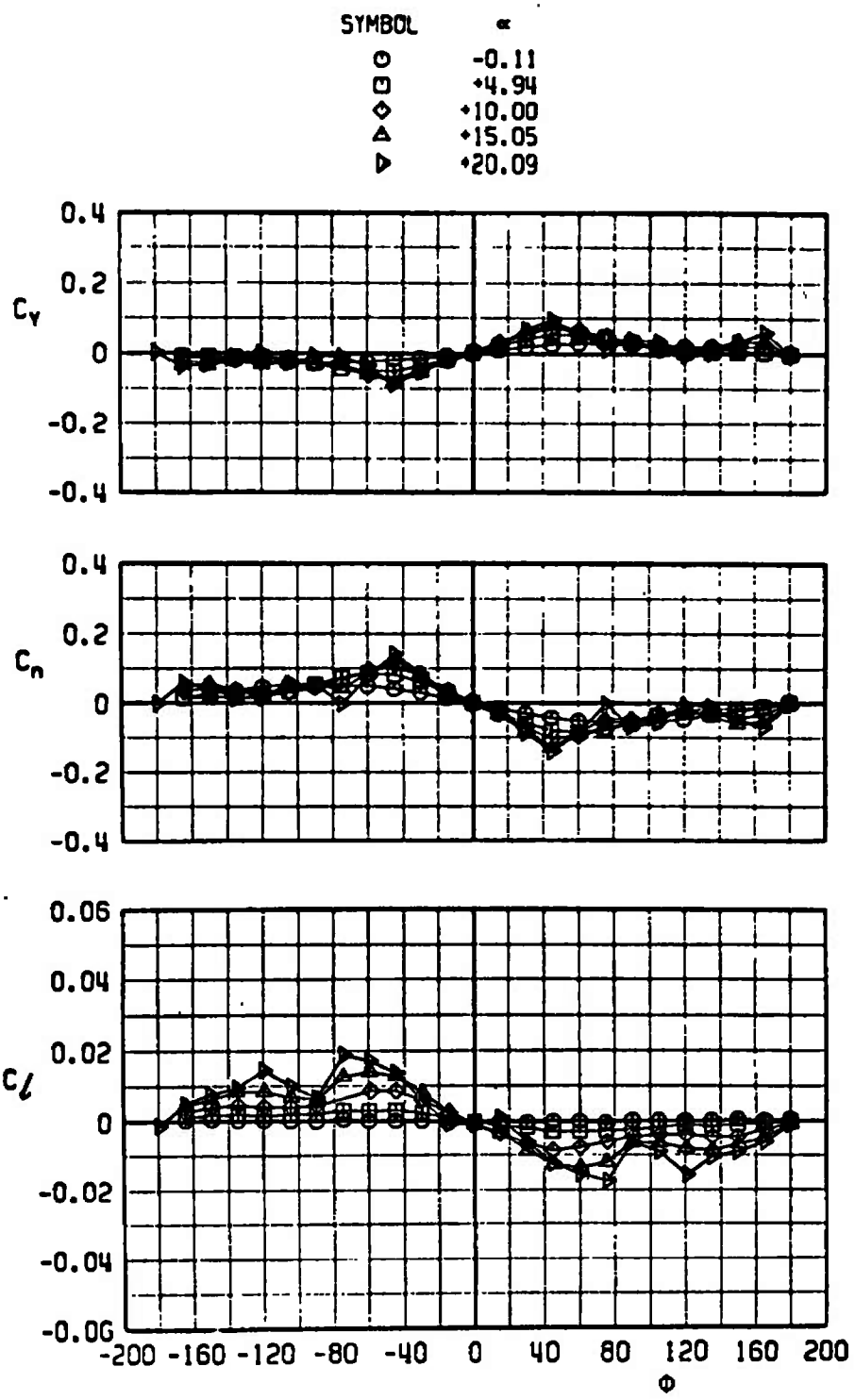

a. $M_\infty = 0.3$

Fig. 7 Variation of C_Y, C_n, and C_ℓ with Roll Angle for Configuration $B_S N_{S2} A_{S1} F_{S2}$

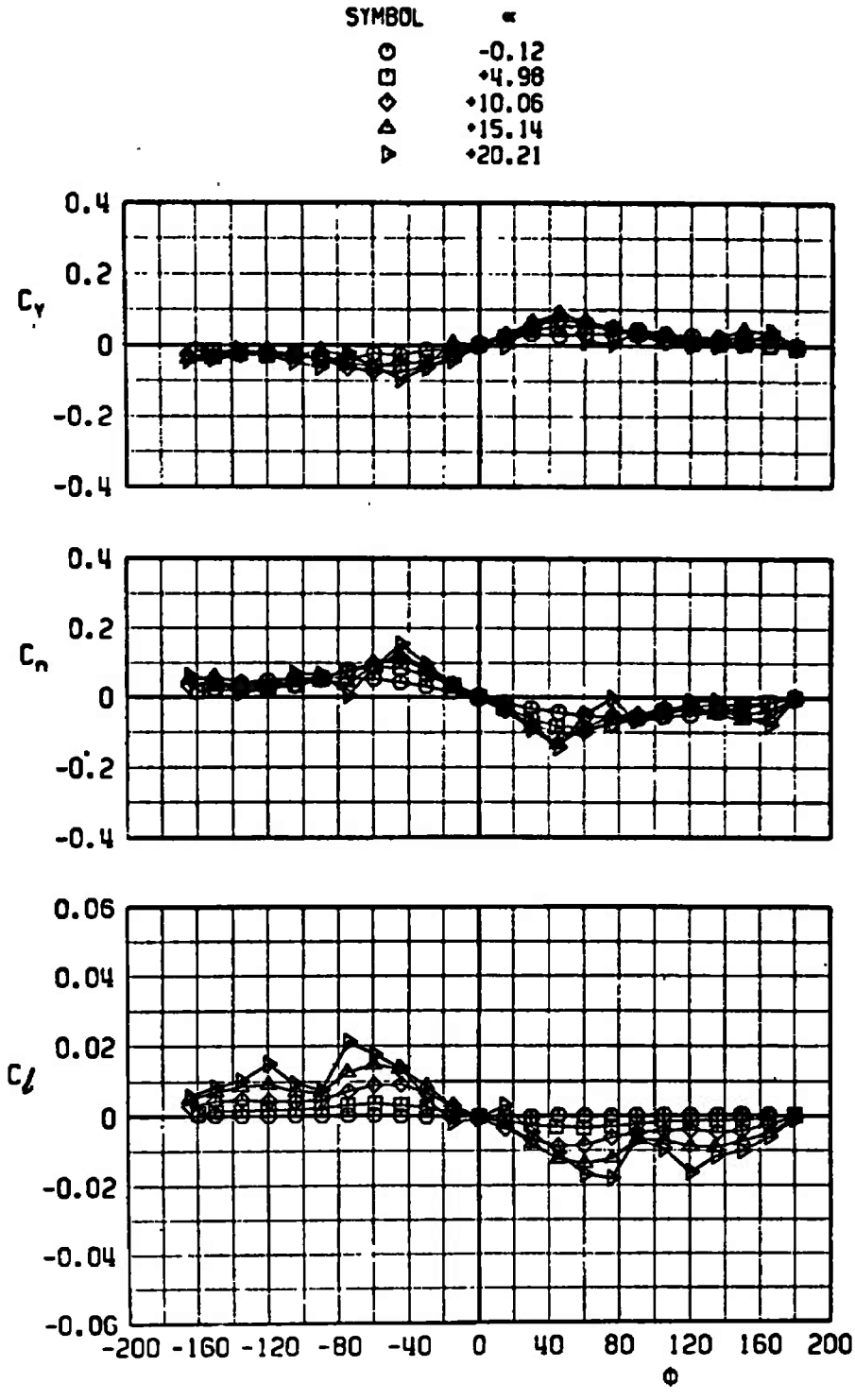

b. $M_\infty = 0.5$

Fig. 7 Continued

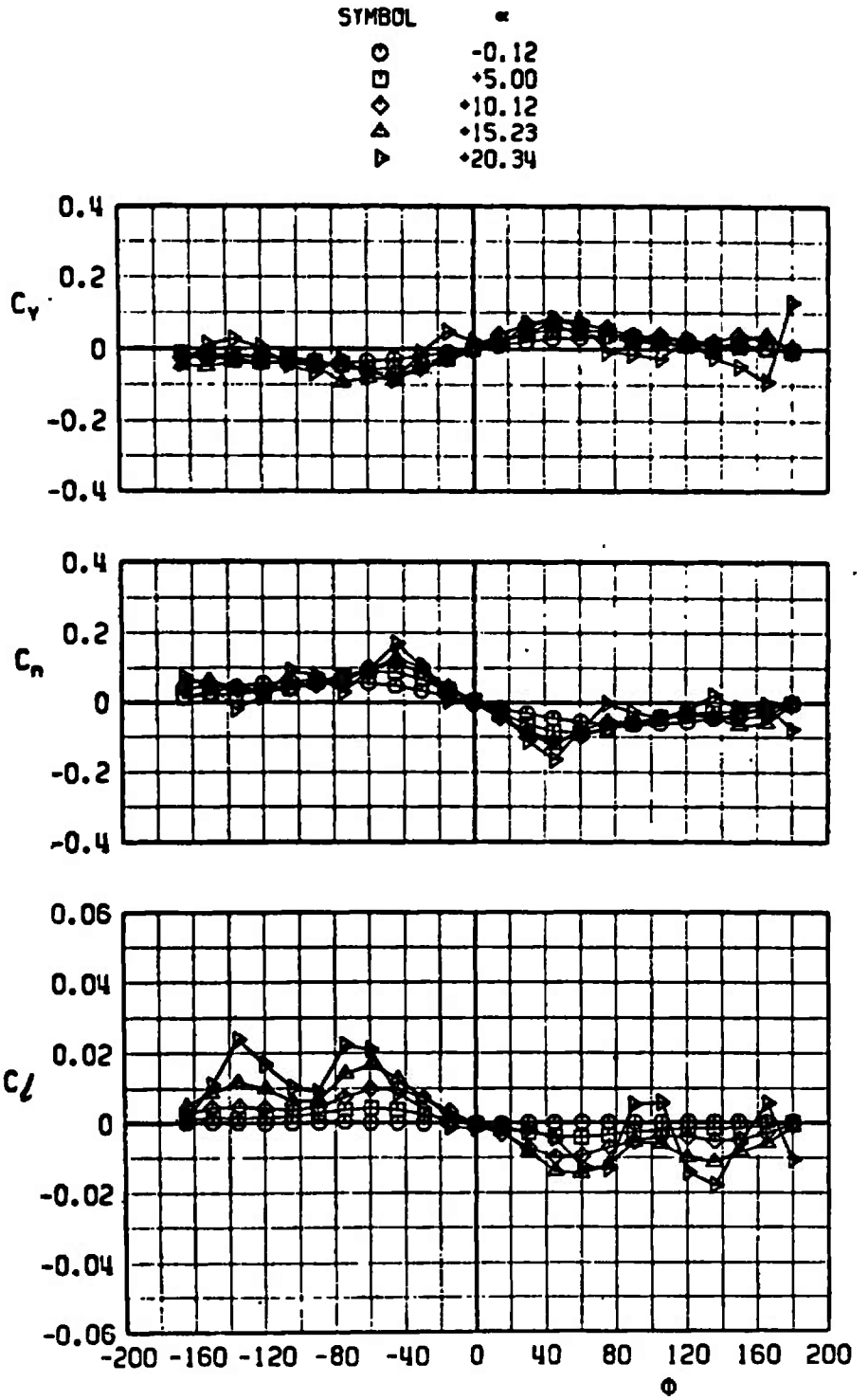

c. $M_\infty = 0.7$
Fig. 7 Continued

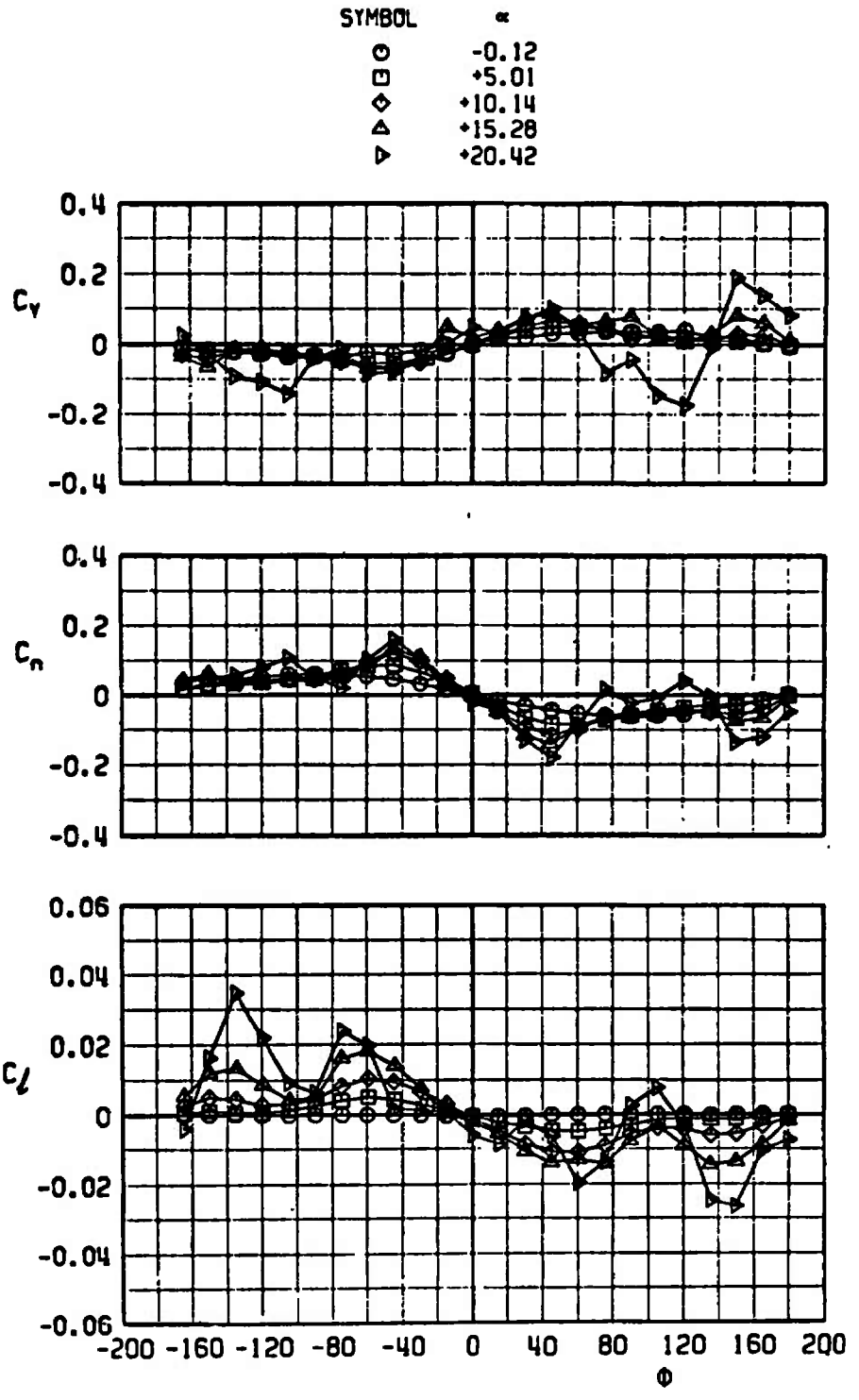

d. $M_\infty = 0.8$

Fig. 7 Continued

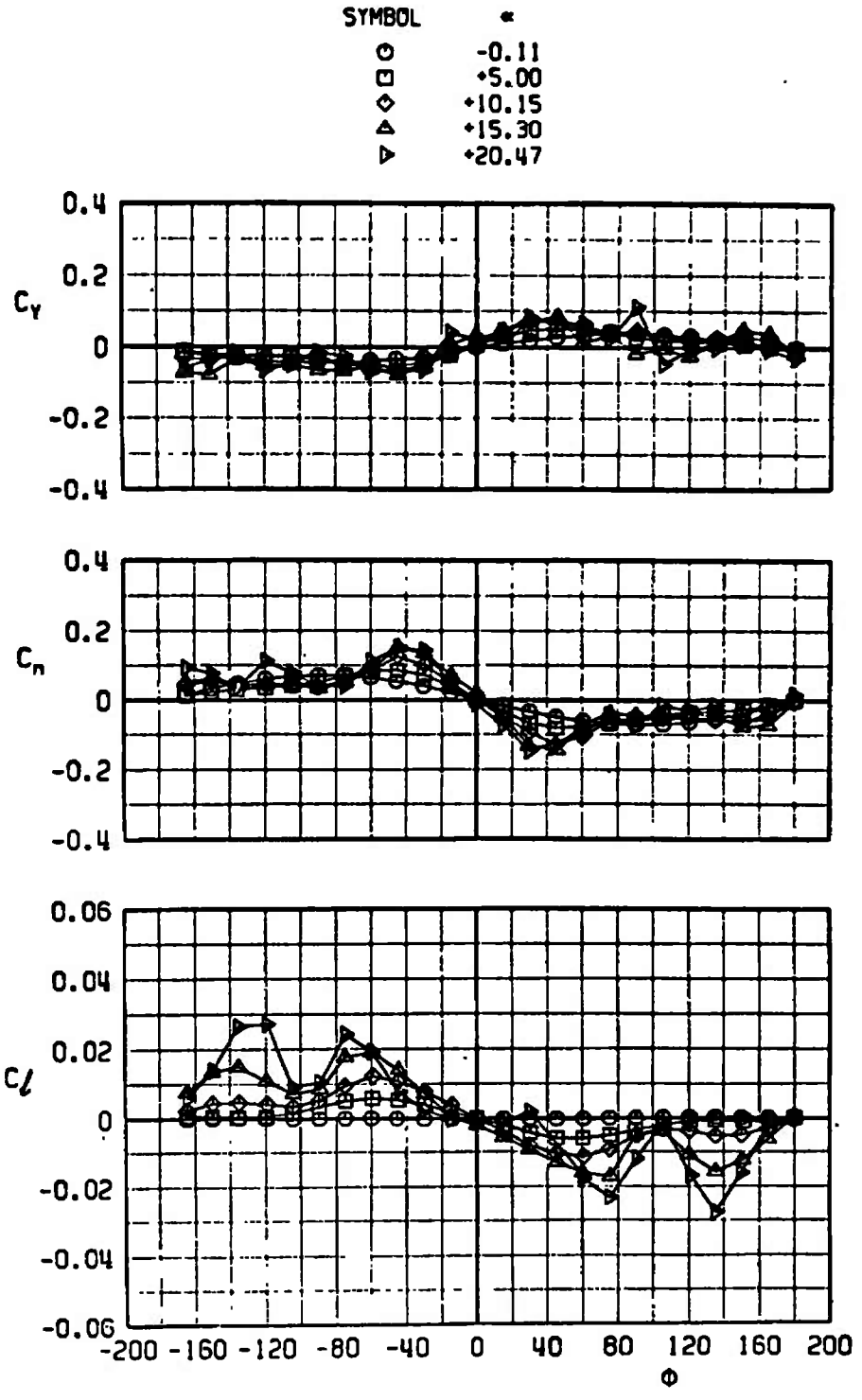

e. $M_\infty = 0.9$

Fig. 7 Continued

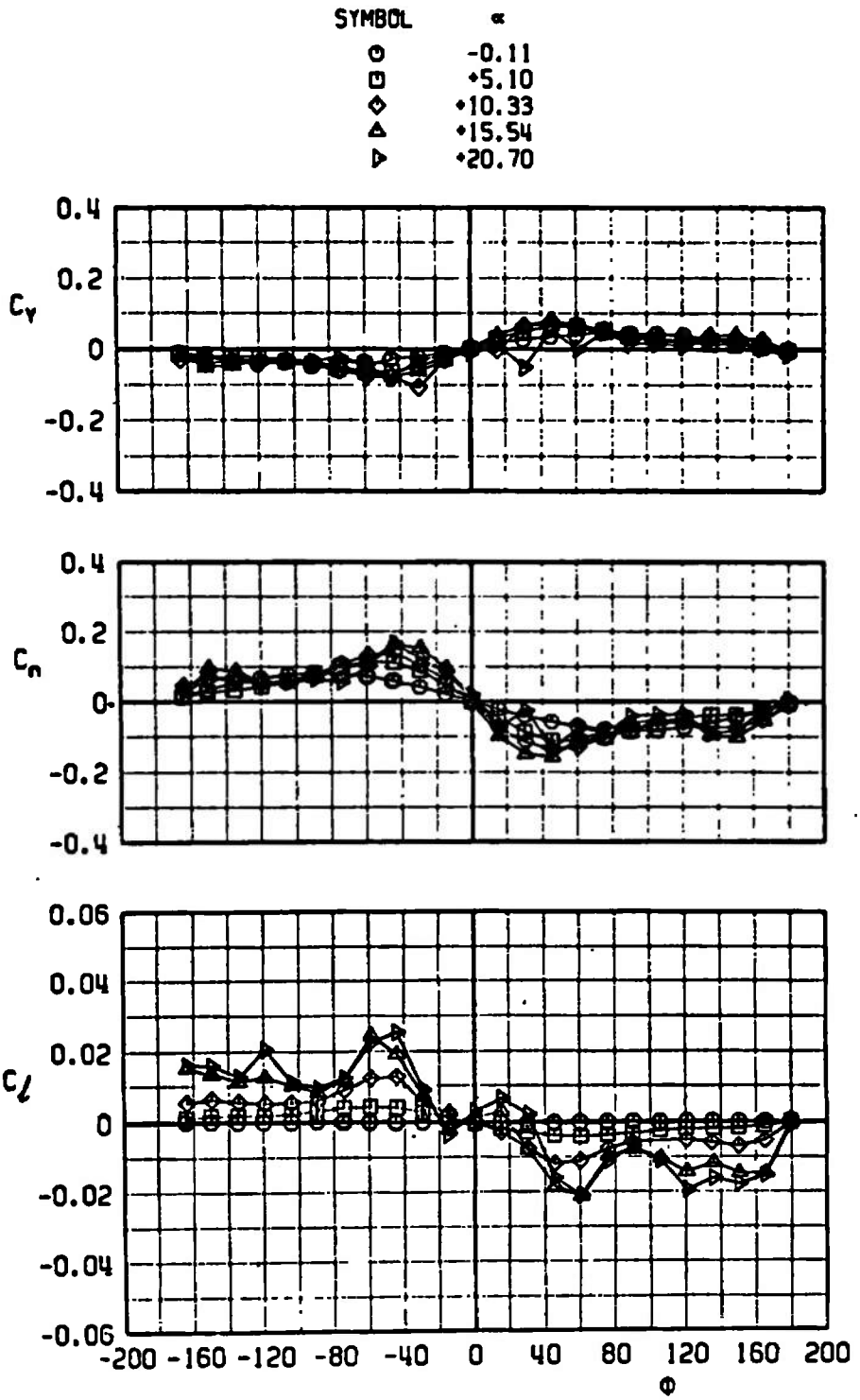

f. $M_\infty = 1.1$

Fig. 7 Continued

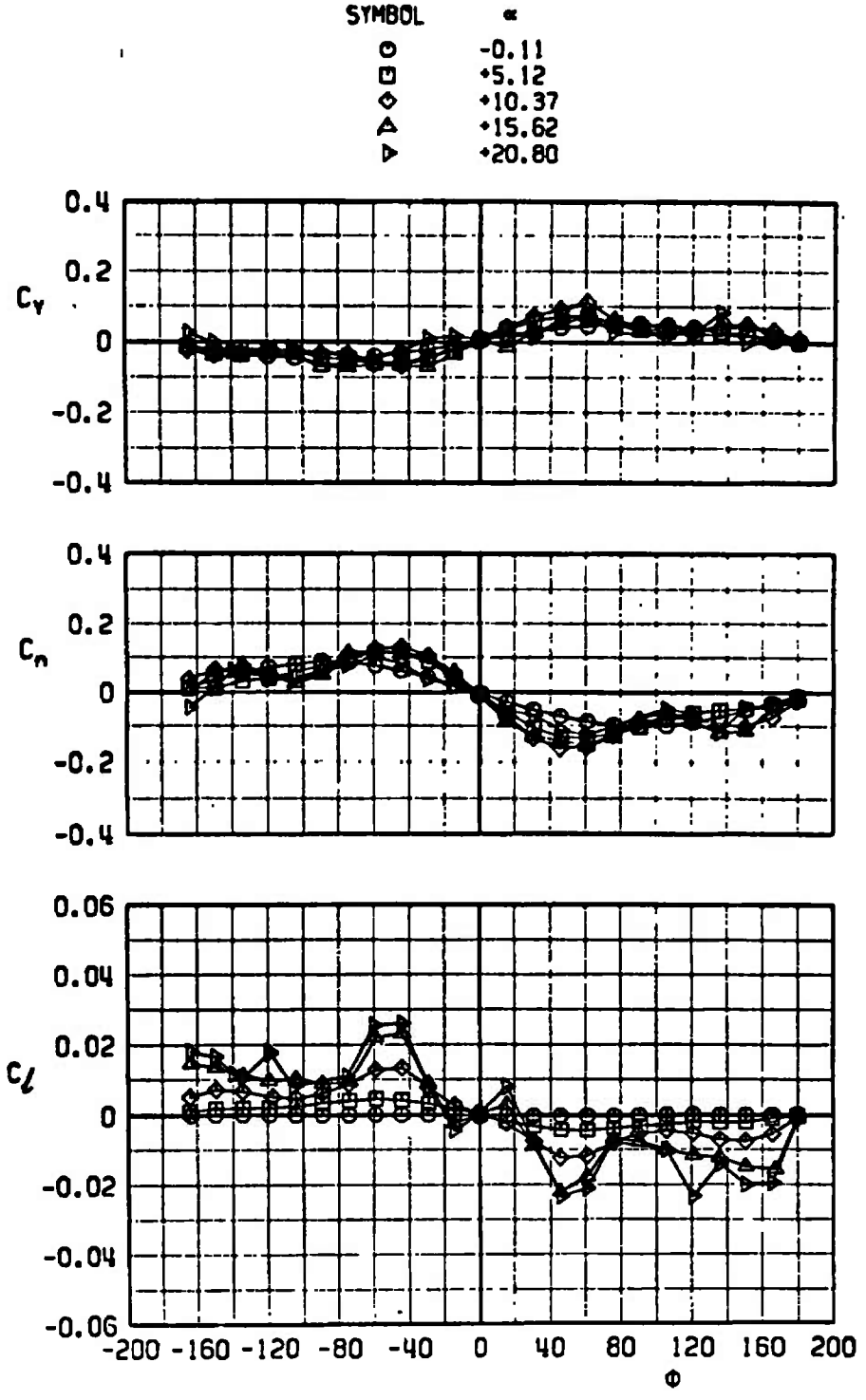

g. $M_\infty = 1.2$

Fig. 7 Concluded

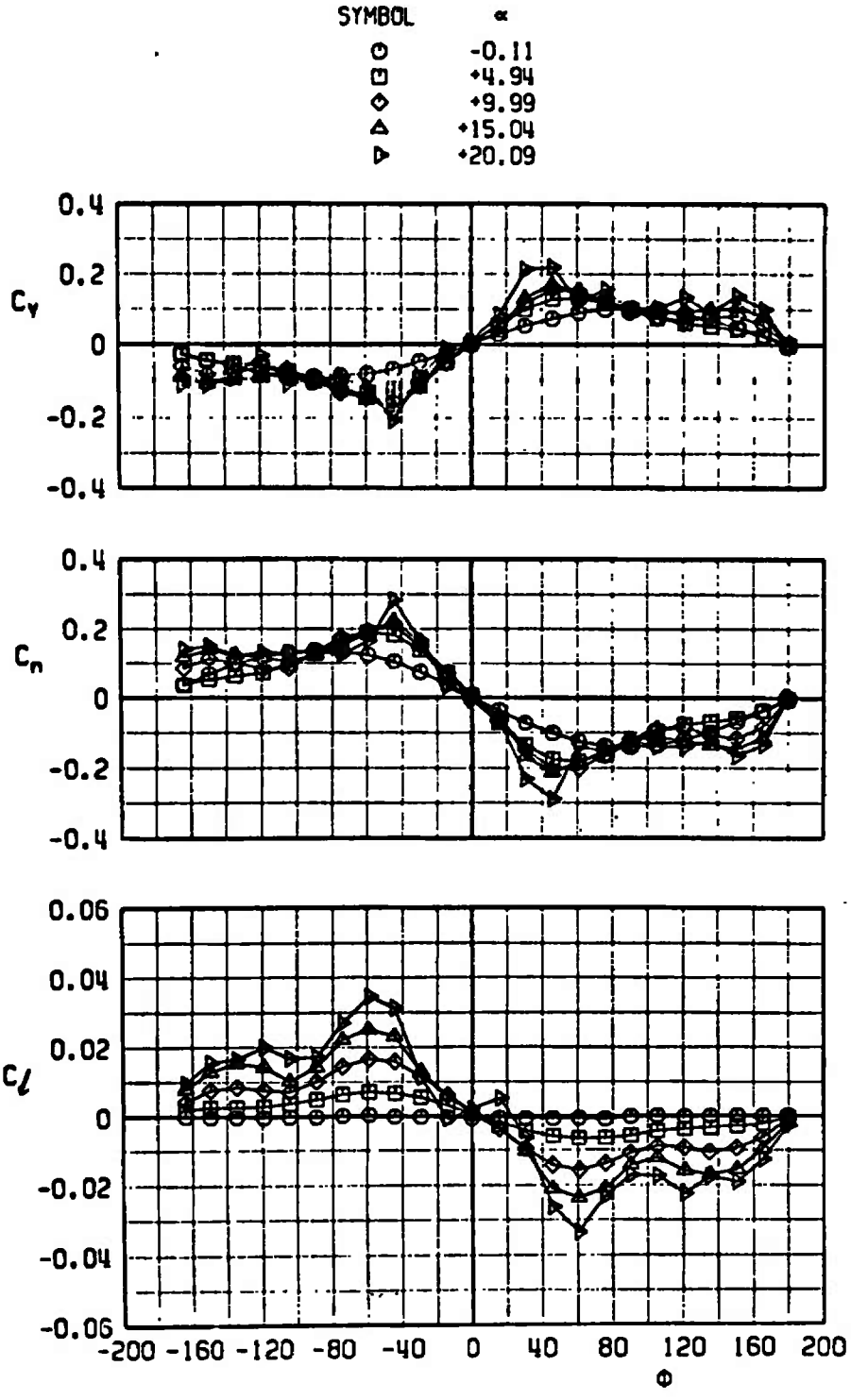

a. $M_\infty = 0.3$

Fig. 8 Variation of C_Y, C_n and C_ℓ with Roll Angle for Configuration $B_S N_{S2} A_{S1} F_{S5}$

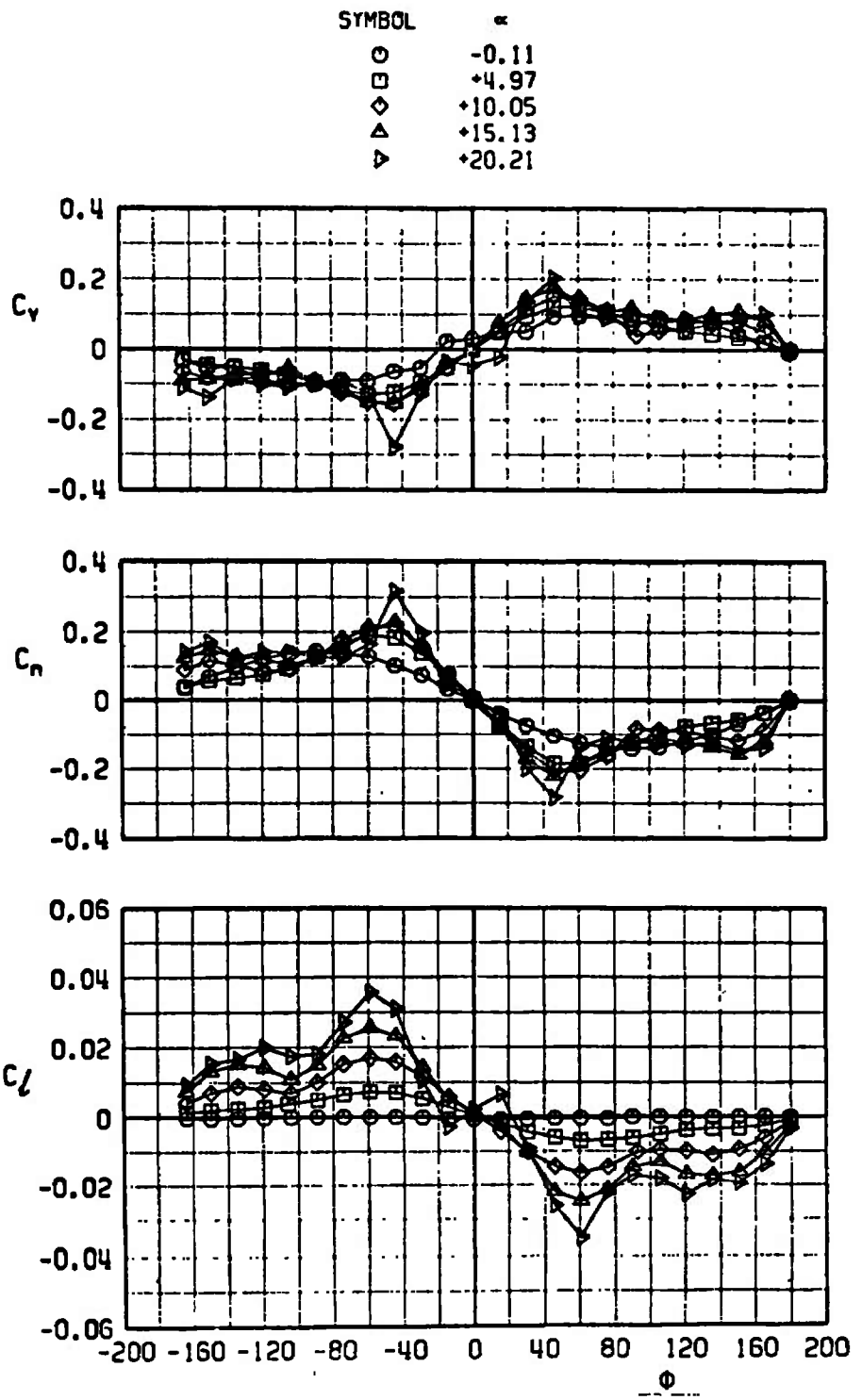

b. $M_\infty = 0.5$

Fig. 8 Continued

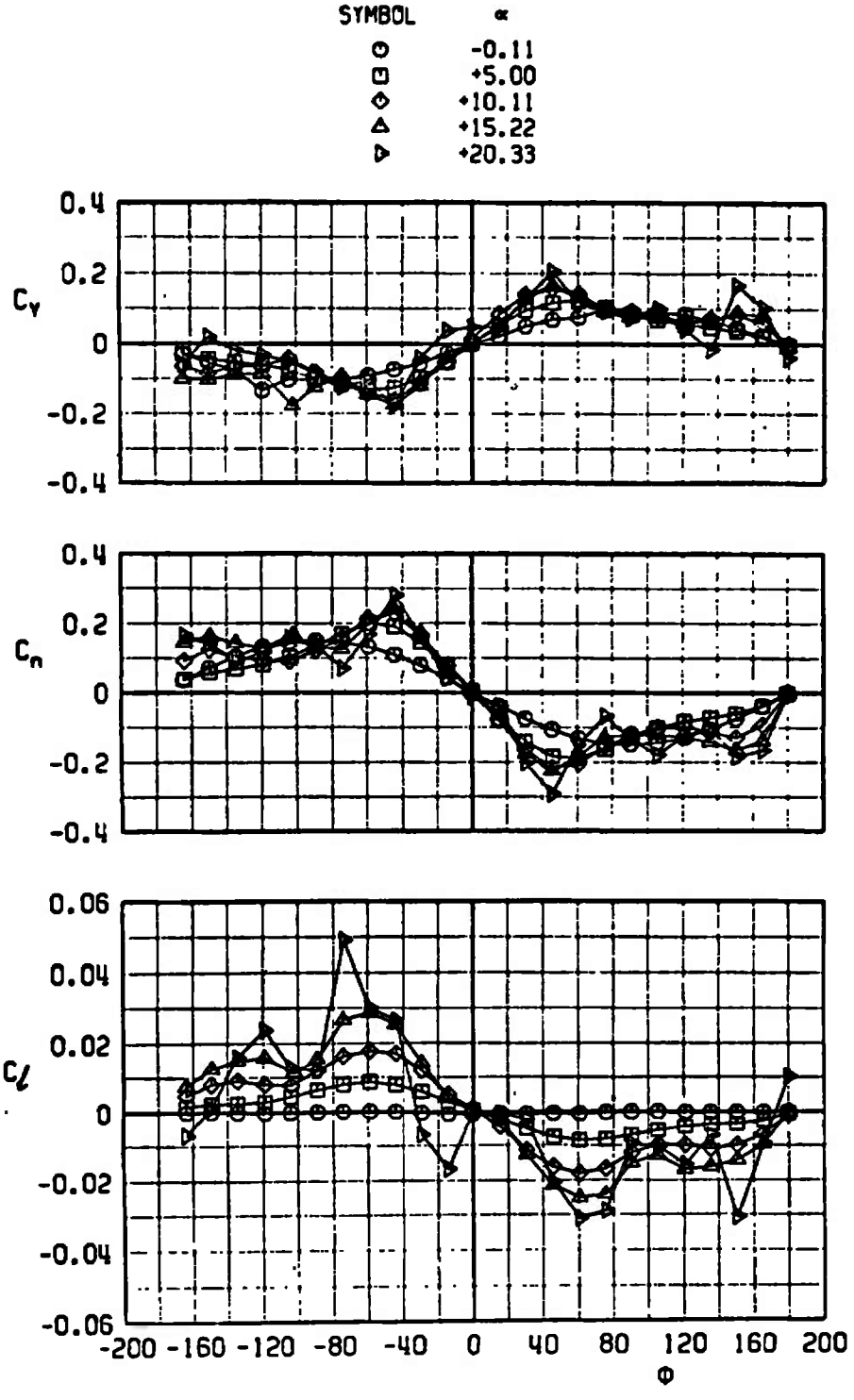

c. $M_\infty = 0.7$

Fig. 8 Continued

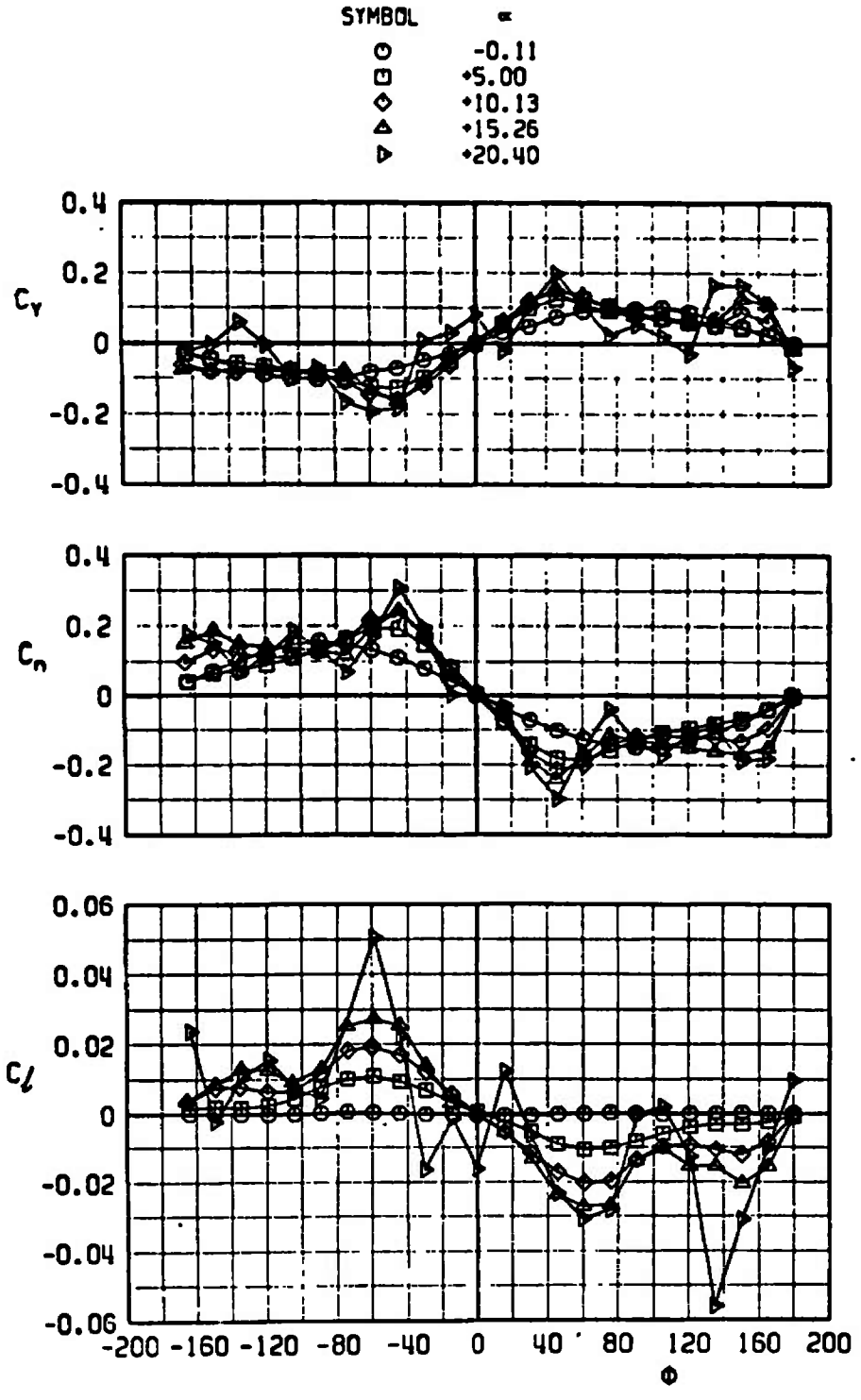

d. $M_\infty = 0.8$

Fig. 8 Continued

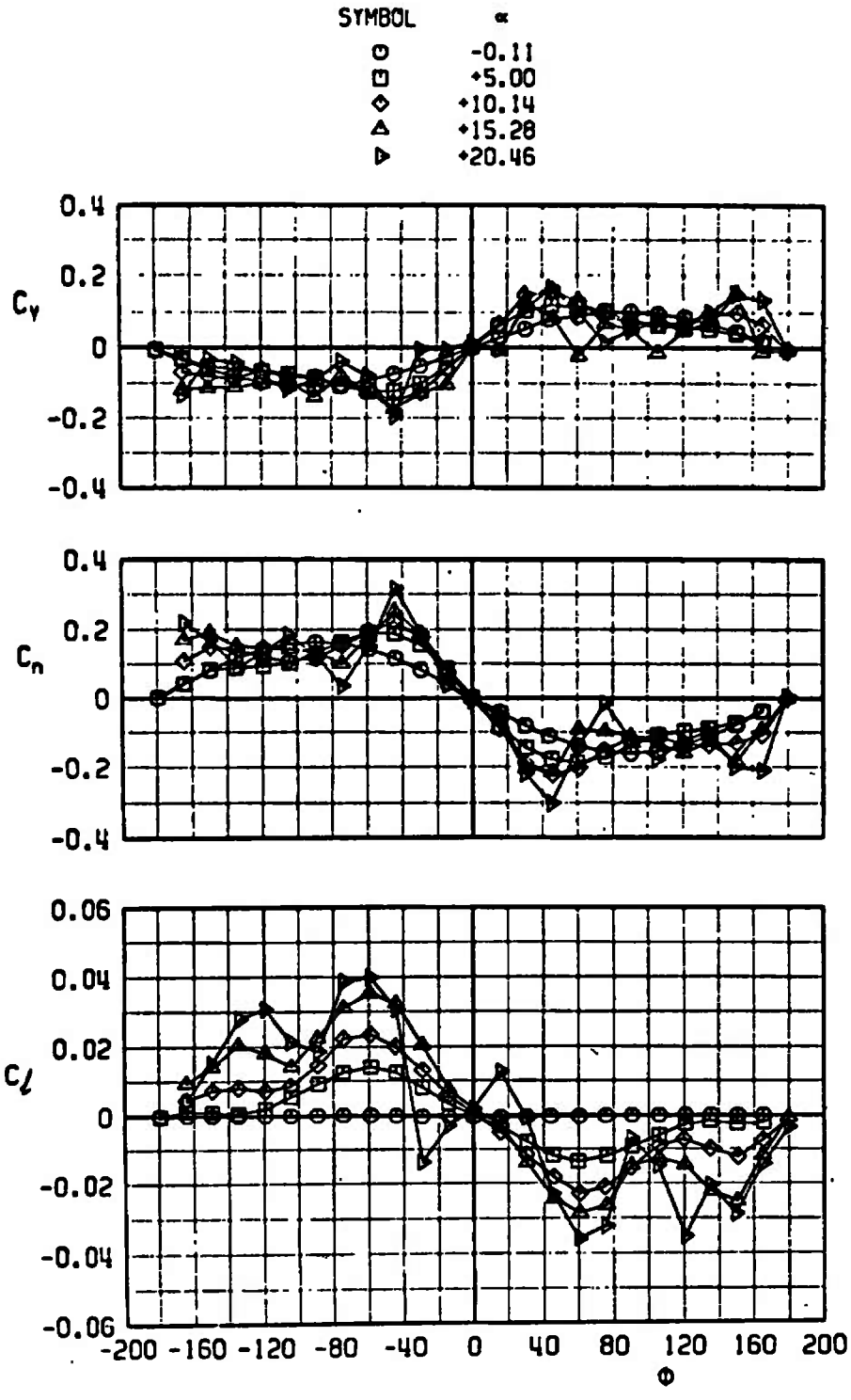

e. $M_\infty = 0.9$

Fig. 8 Continued

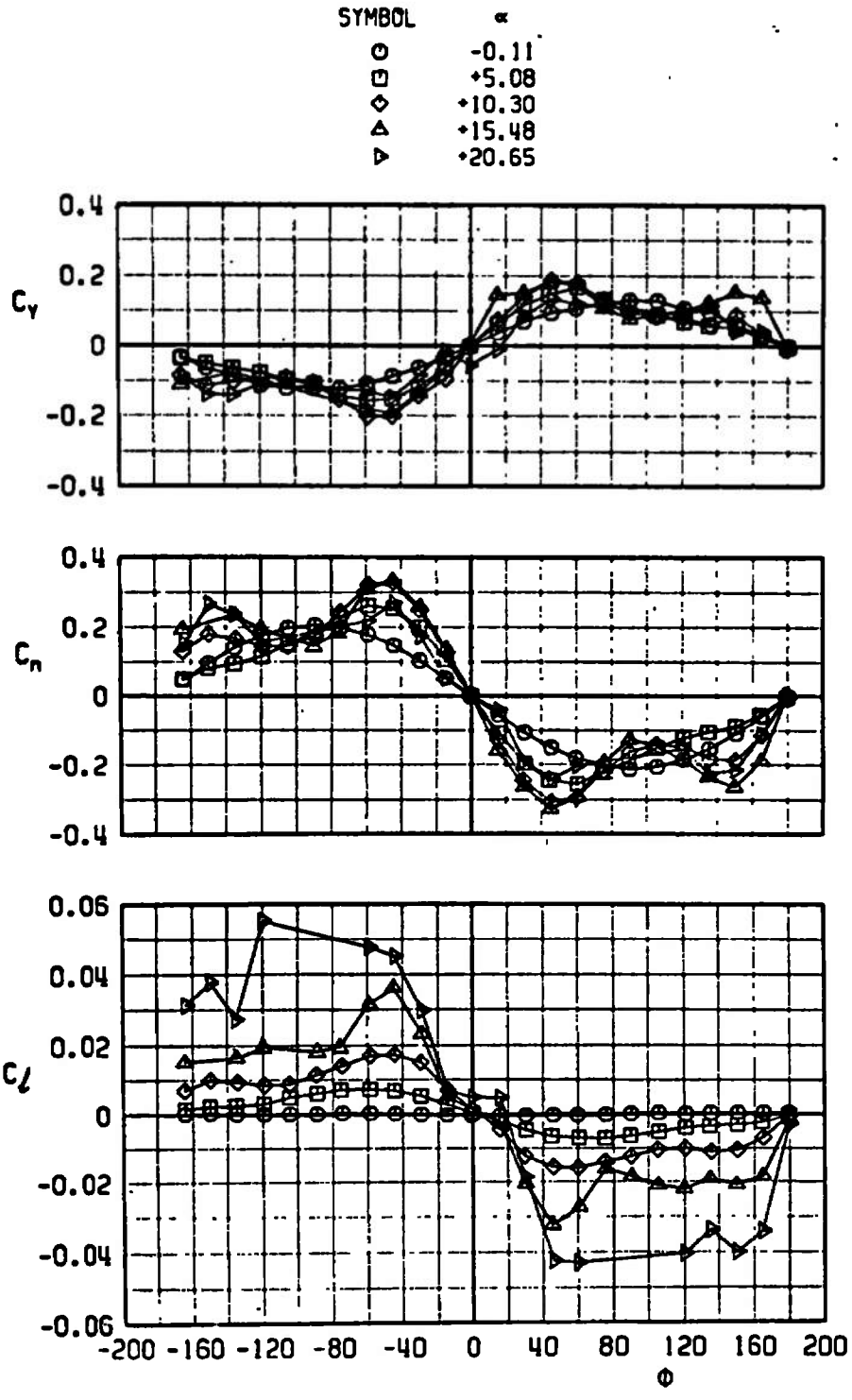

f. $M_\infty = 1.1$
Fig. 8 Continued

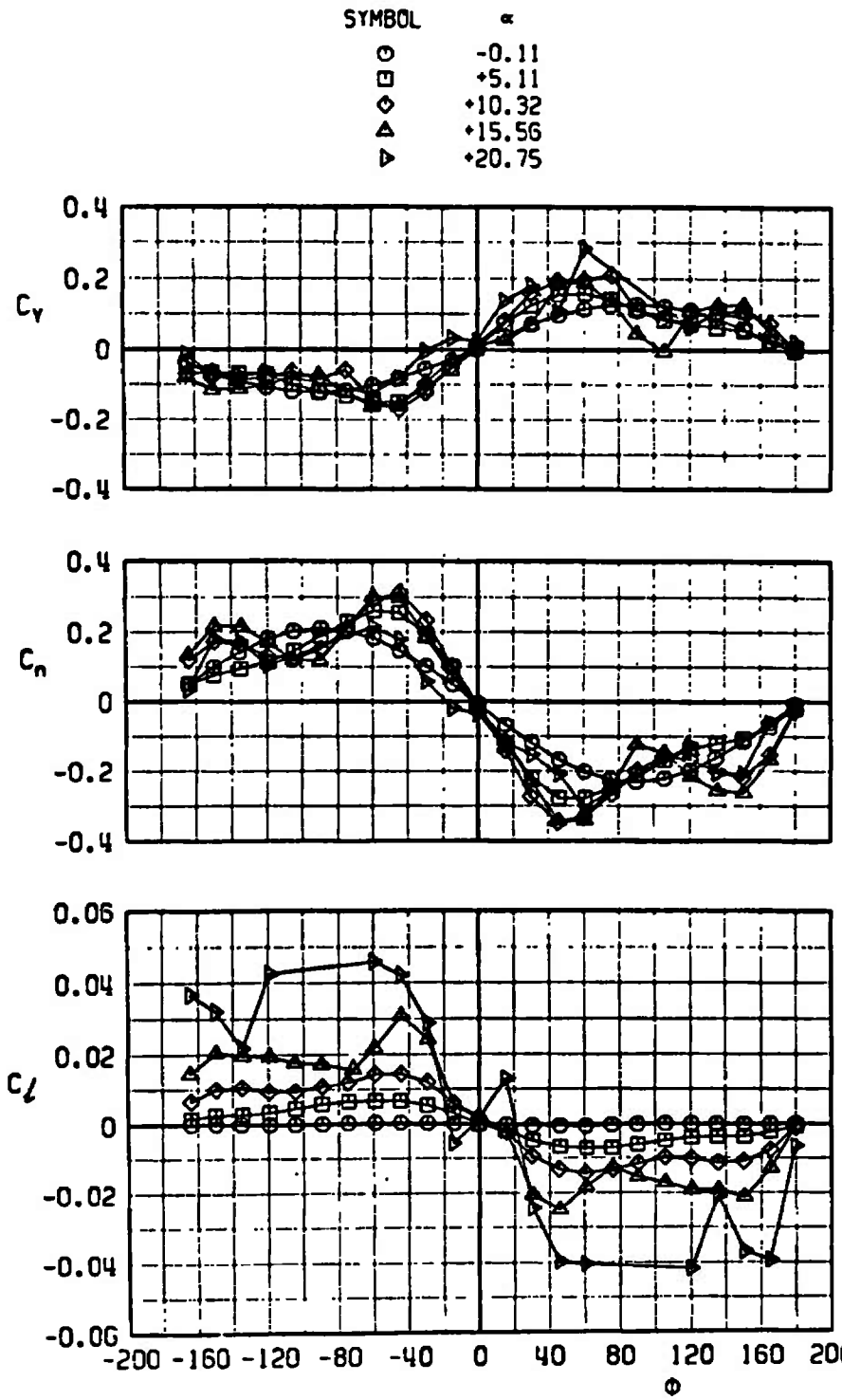

g. $M_\infty = 1.2$

Fig. 8 Concluded

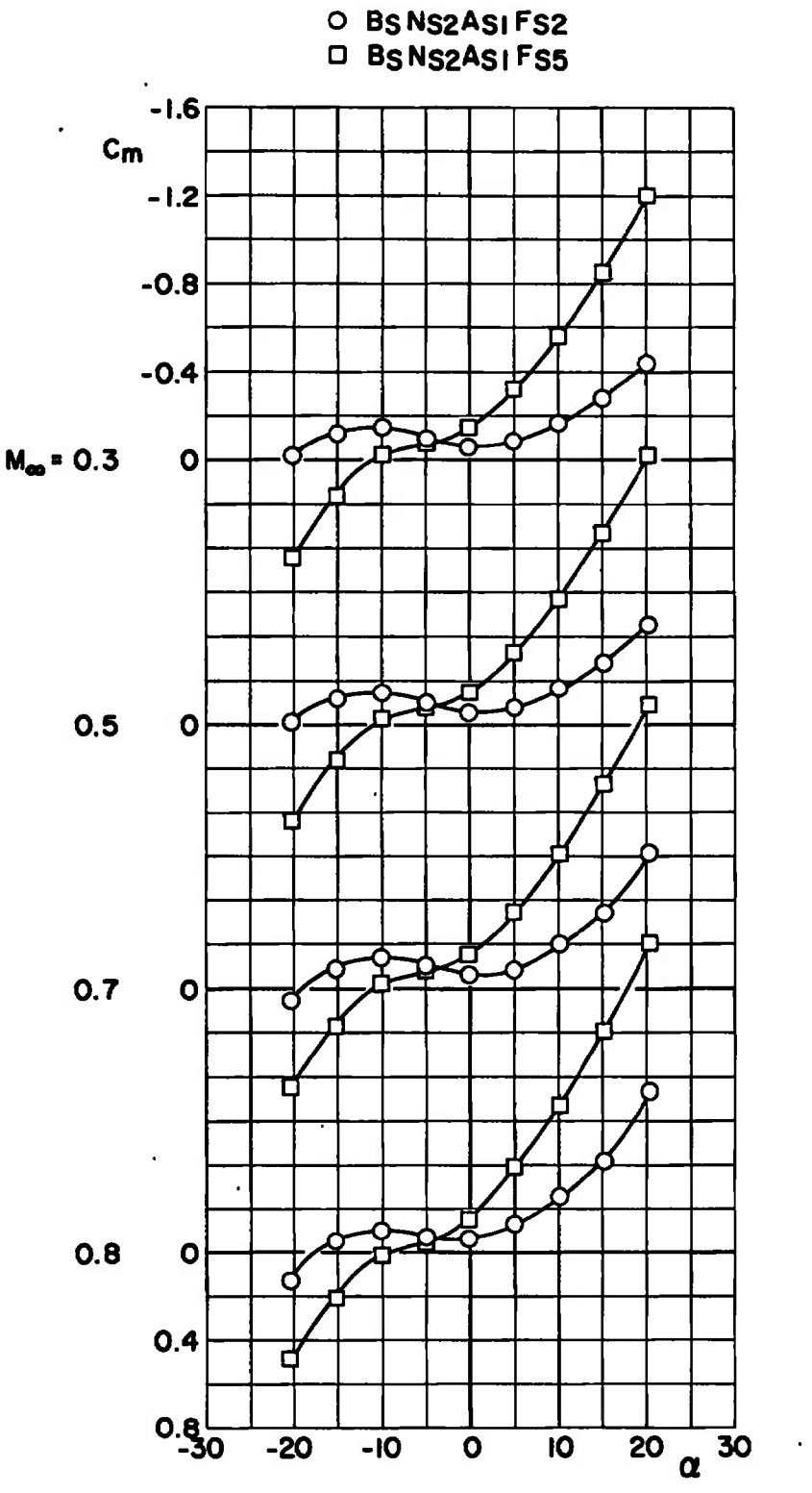

a. M_∞ = 0.3 to 0.8

Fig. 9 Effects of Fin Span on Pitching-Moment Coefficients, ϕ = 0

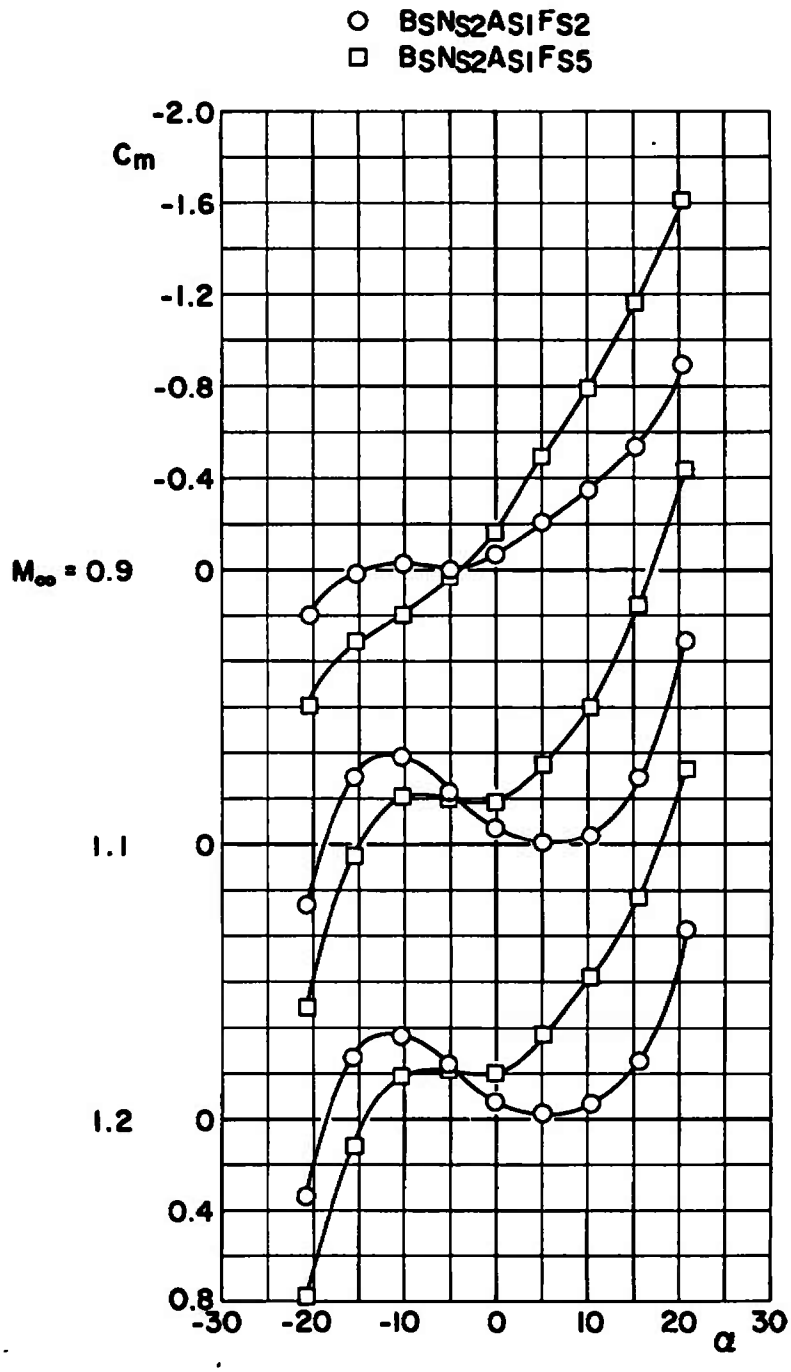

b. M_∞ = 0.9 to 1.2

Fig. 9 Concluded

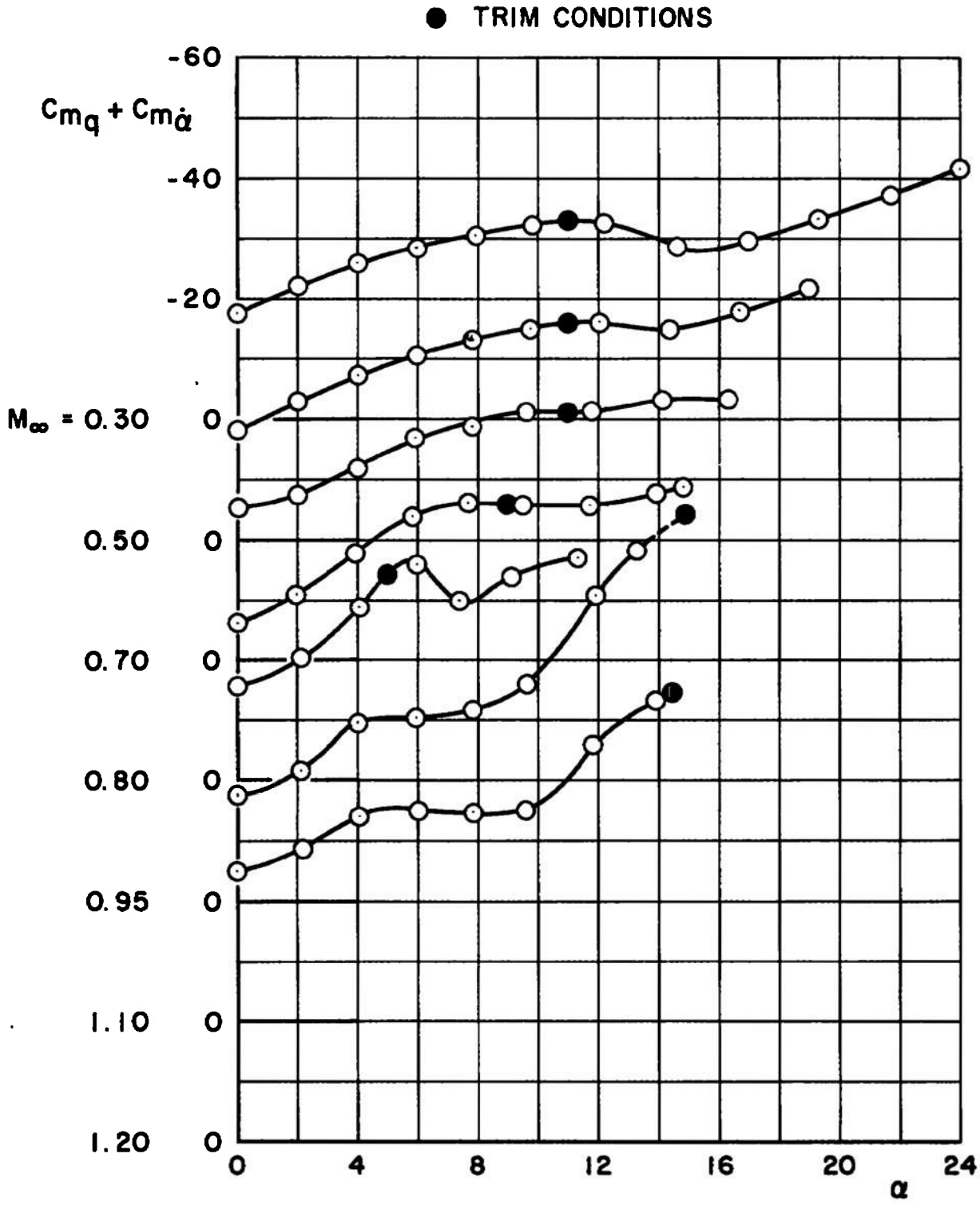

Fig. 10 Variation of $C_{m_q} + C_{m_{\dot{\alpha}}}$ with Angle of Attack, $B_S N_{S2} A_{S1} F_{S5}$, $\delta_F = 0$

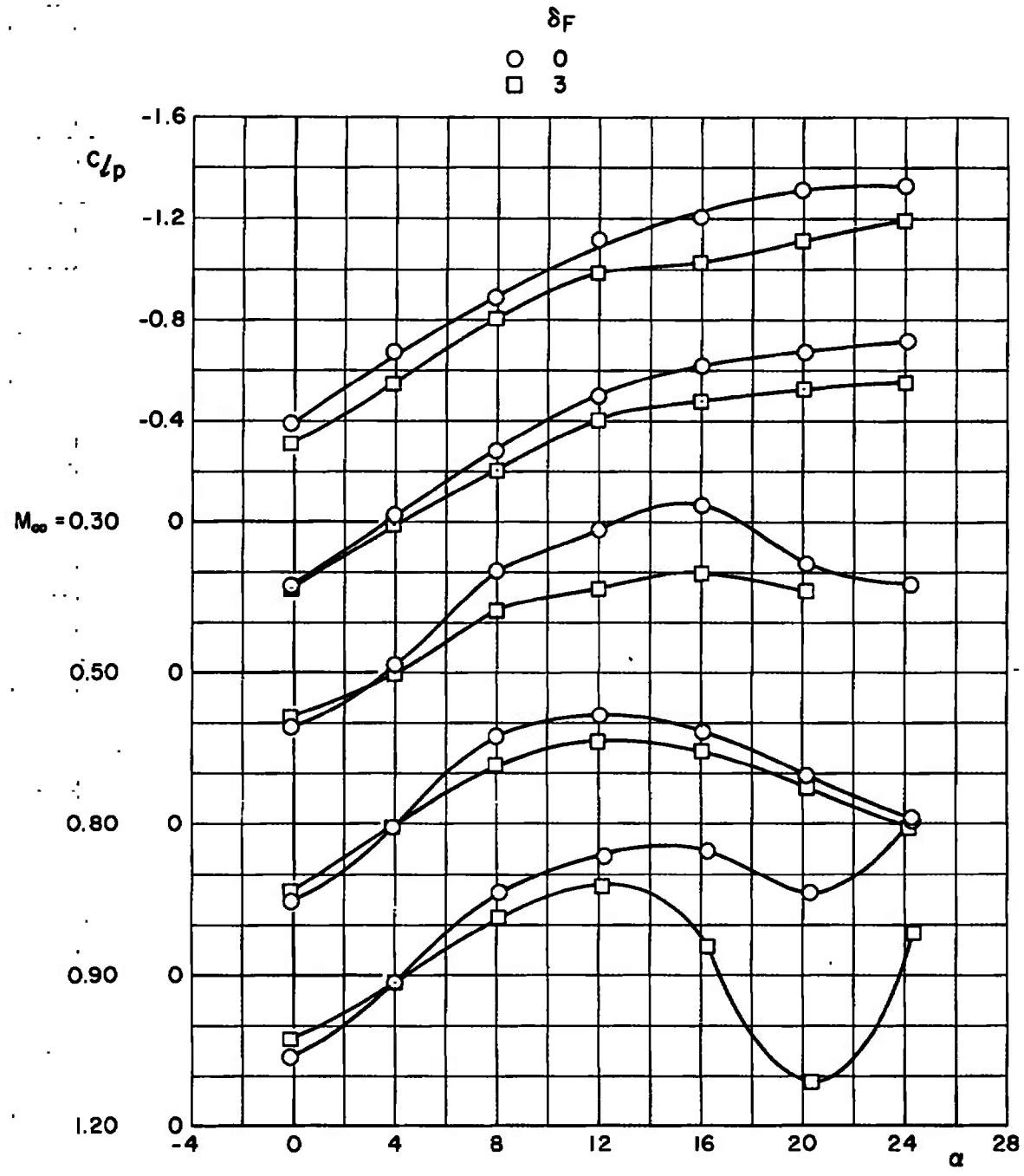

Fig. 11 Effects of Fan Cant on Roll-Damping Coefficient, $B_S N_{S2} A_{S1} F_{S5}$

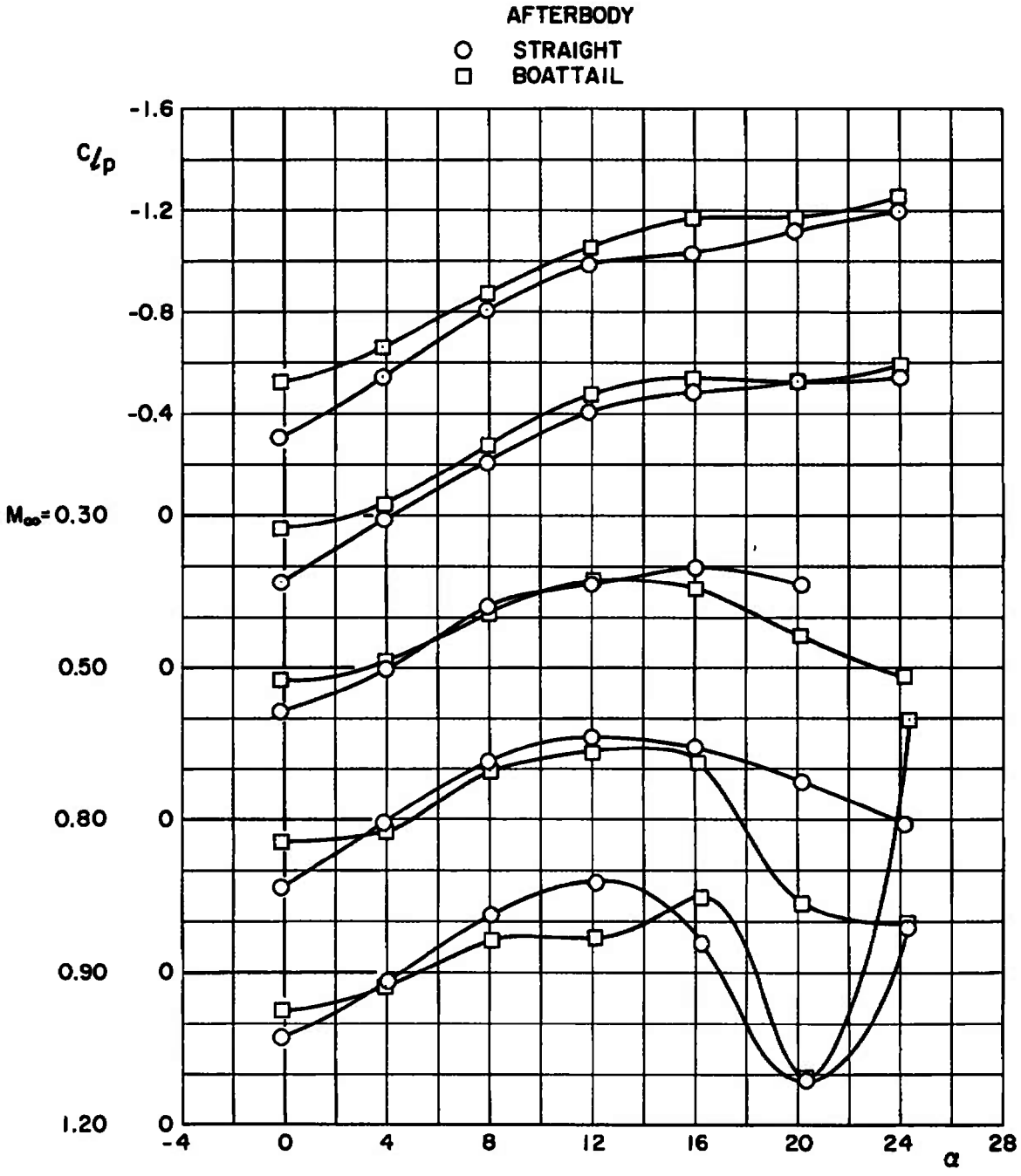

a. C_{ℓ_p} versus $\dot{\alpha}$

Fig. 12 Effects of Afterbody Shape on Roll-Damping Characteristics, $B_S N_{S2} A_{1,2} F_{S5}$, $\delta_F = 3$

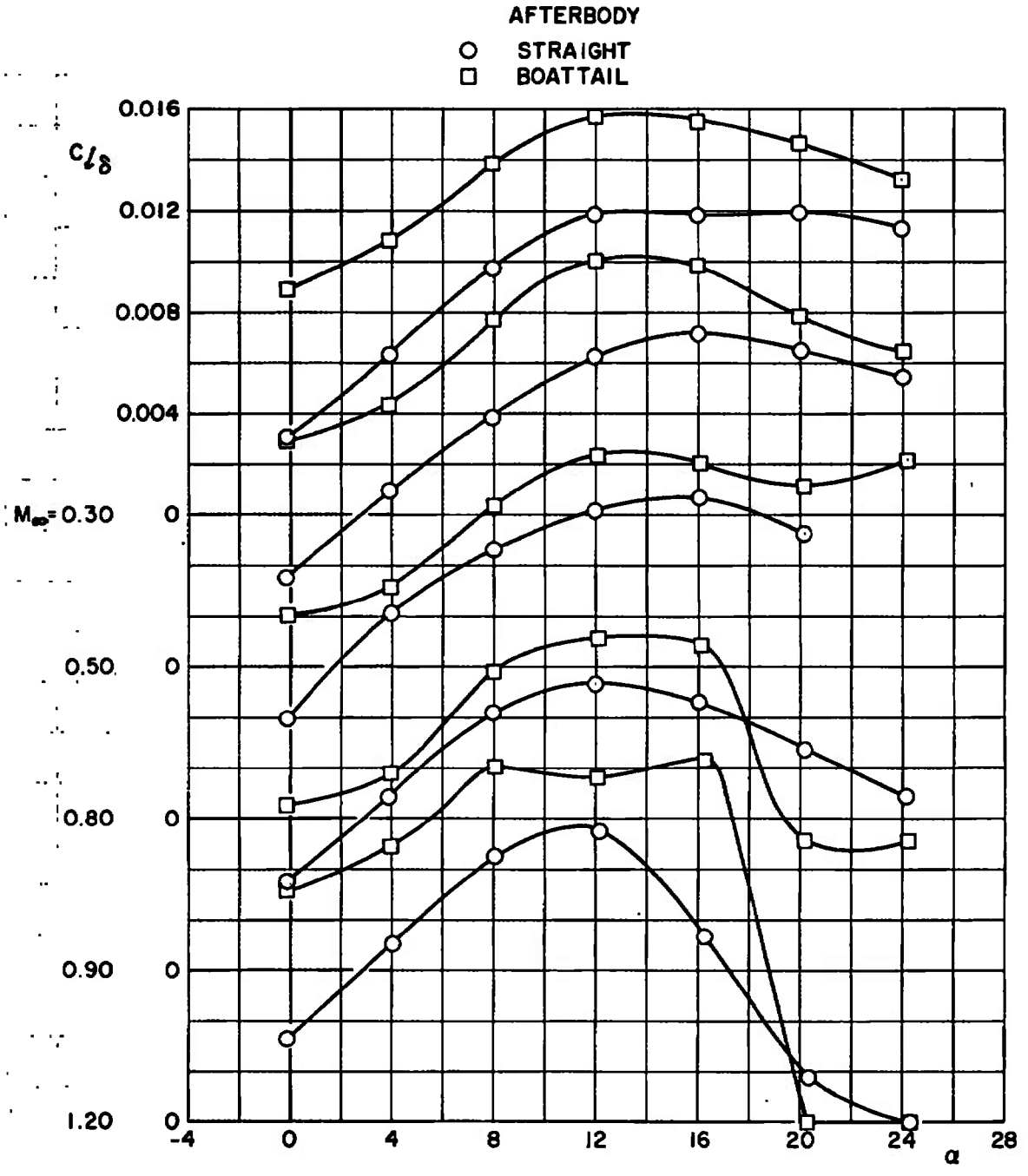

b. C_{l_δ} versus α
Fig. 12 Concluded

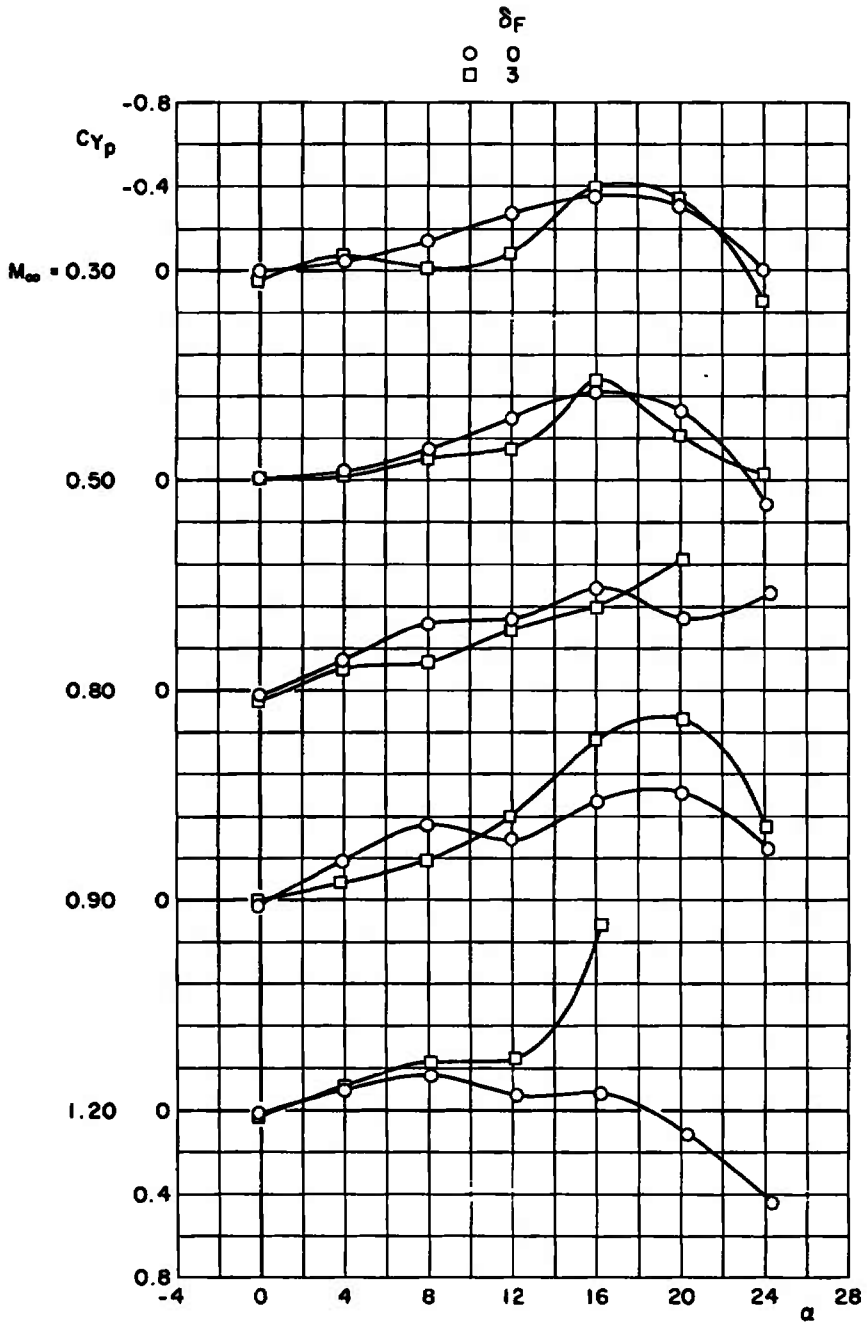

a. C_{Y_p} versus α

Fig. 13 Effects of Fin Cant on Magnus Characteristics, $B_S N_{S2} A_{A1} F_{S6}$

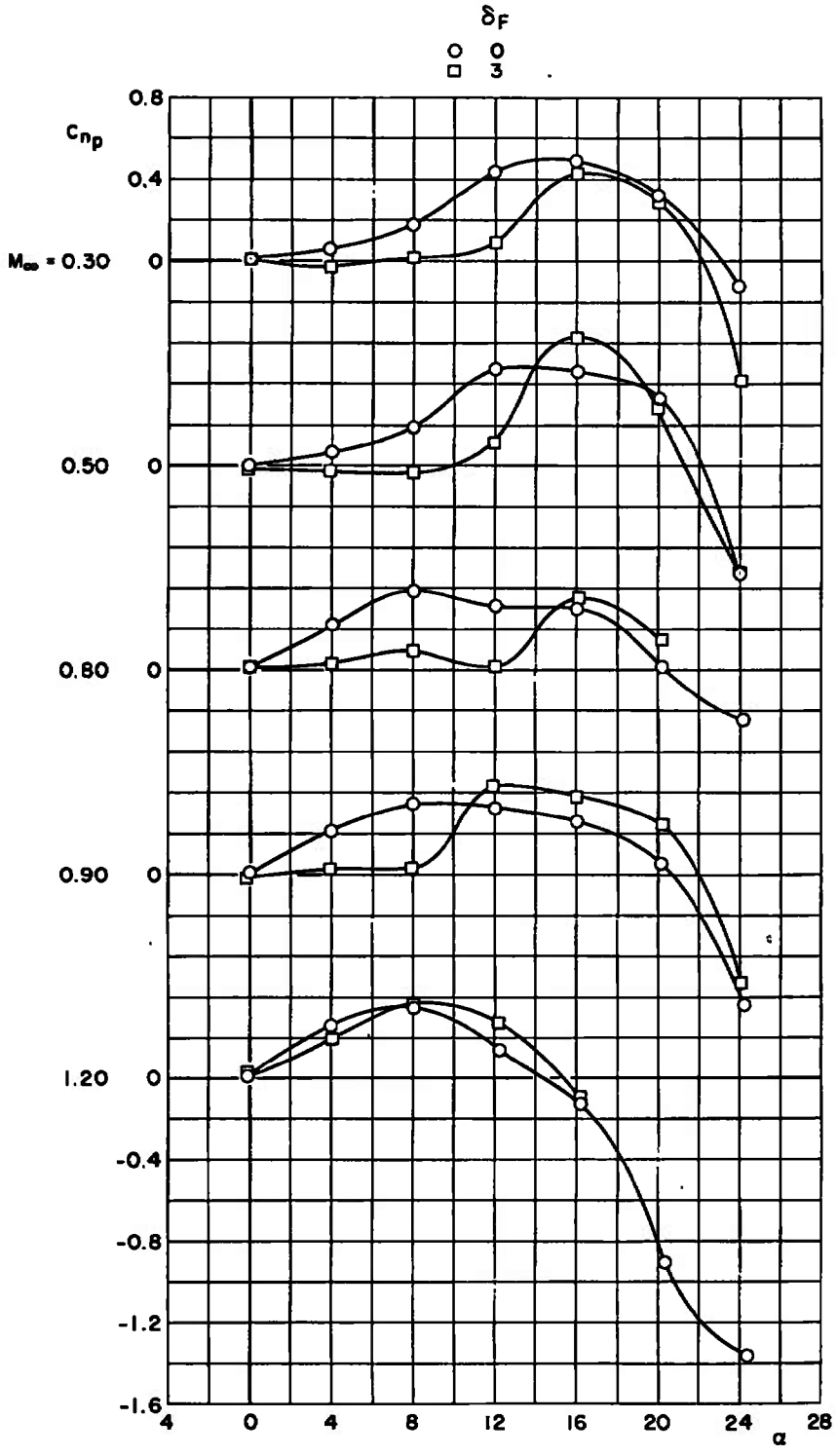

b. C_{n_p} versus $\dot{\alpha}$
Fig. 13 Concluded

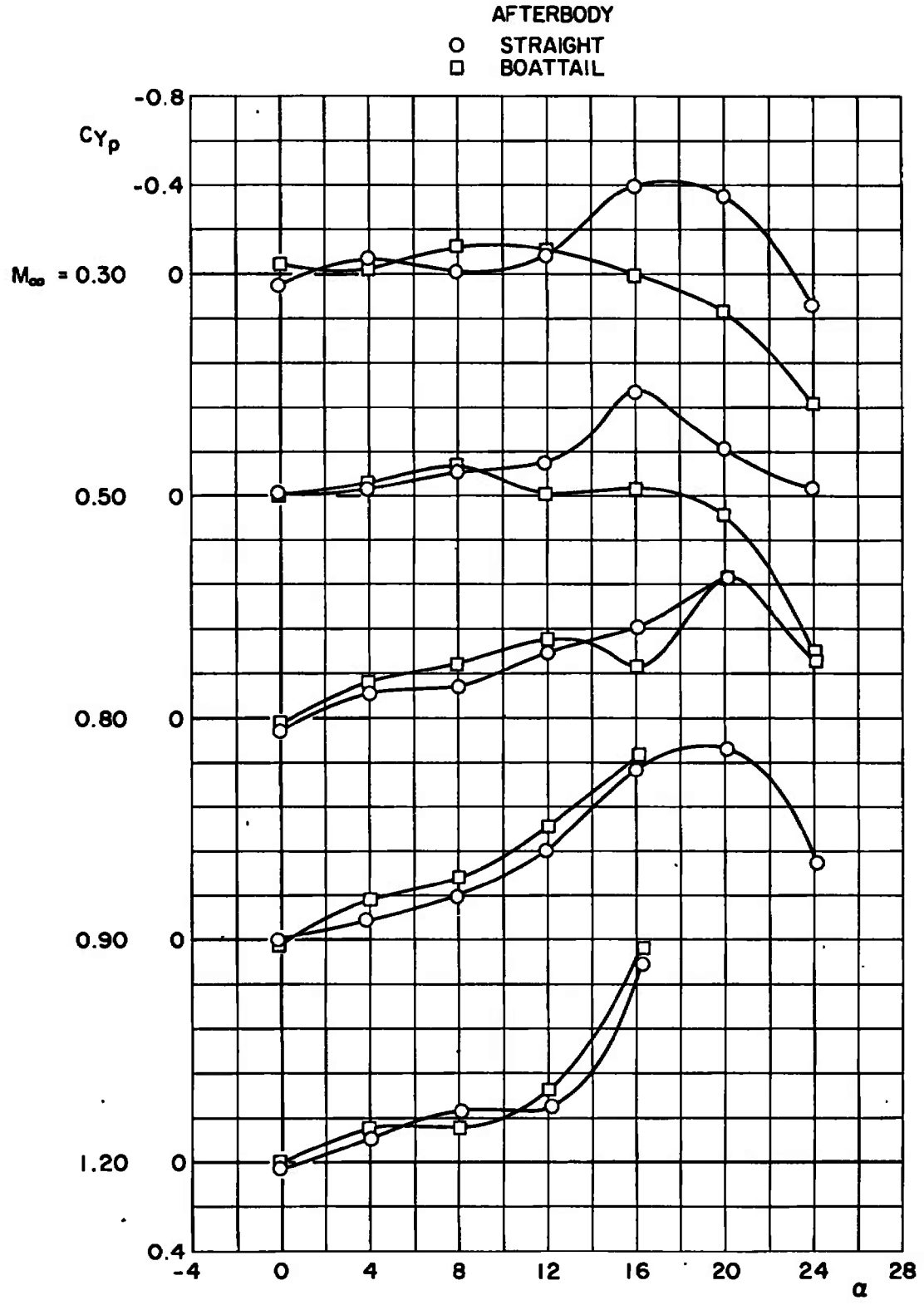

a. C_{Y_p} versus $\dot{\alpha}$

Fig. 14 Effects of Afterbody Shape on Magnus Characteristics, $B_S N_{S2} A_{S1,2} F_{S5}$, $\delta_F = 3$

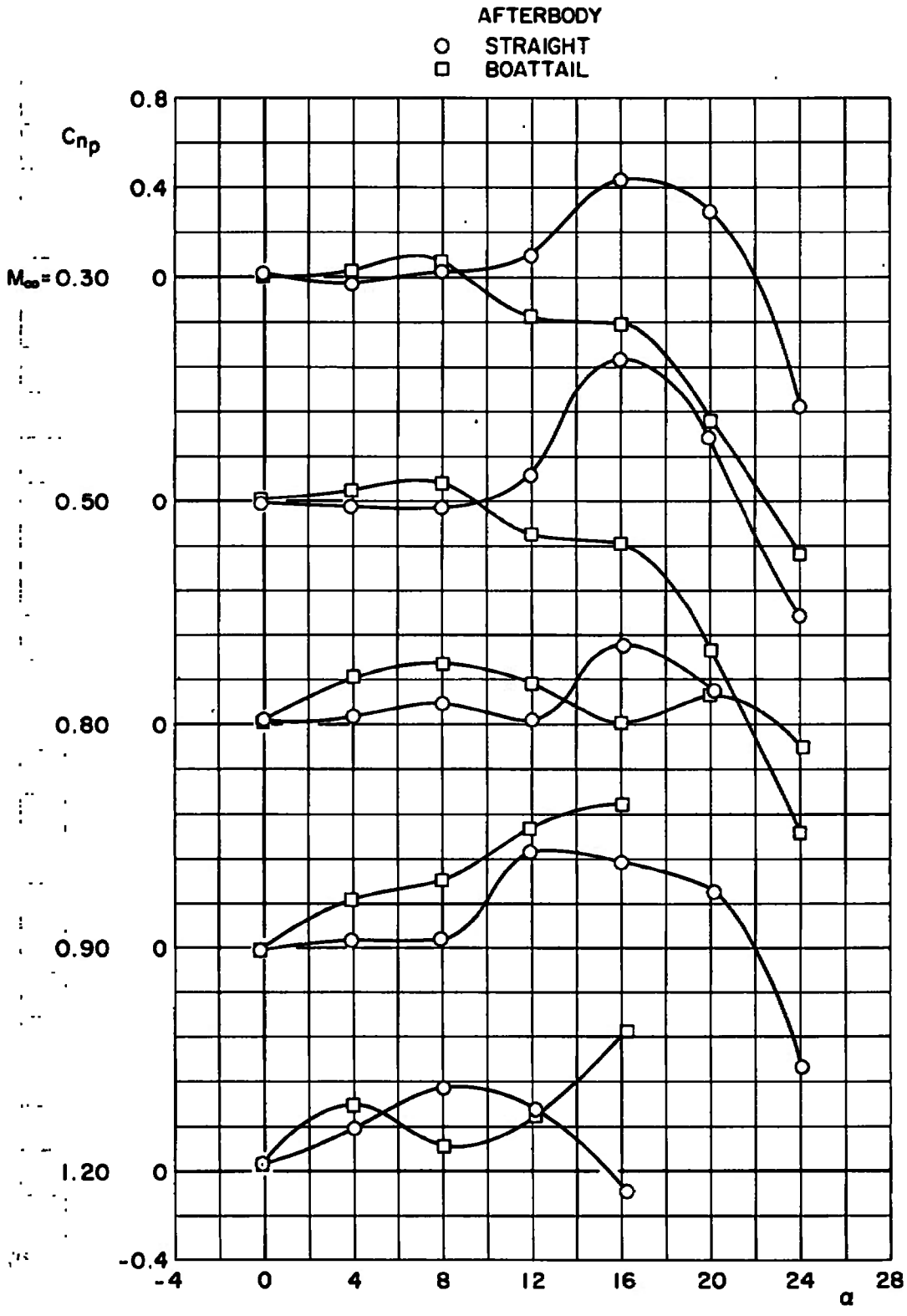

b. C_{n_p} versus α
Fig. 14 Concluded

TABLE I
STATIC STABILITY PHASE TEST CONDITIONS

M_∞	α, deg	ϕ, deg	Re/ft x 10^{-6}	q_∞, lb/ft^2
0.3	-0.11 to 20.09	-165 to 180	2.2	154
0.5	-0.12 to 20.21	↓	↓	242
0.7	-0.12 to 20.34	↓	↓	322
0.8	-0.12 to 20.42	↓	↓	356
0.9	-0.11 to 20.47	↓	↓	382
1.1	-0.11 to 20.70	↓	↓	430
1.2	-0.11 to 20.80	↓	↓	499

TABLE II
PITCH-DAMPING PHASE TEST CONDITIONS

M_∞	α, deg	ϕ, deg	$\omega d/2V_\infty$	Re/ft x 10^{-6}	V_∞
0.30	0.01 to 24.05	0	0.029	2.2	349
0.50	0.01 to 18.95	↓	0.018	↓	567
0.70	0.02 to 16.34	↓	0.013	↓	771
0.80	0.02 to 14.81	↓	0.012	↓	870
0.95	-0.01 to 11.29	↓	0.010	↓	1022
1.10	-0.03 to 13.25	↓	0.009	↓	1155
1.20	0.05 to 13.88	↓	0.008	↓	1235

TABLE III
ROLL DYNAMICS PHAST TEST CONDITIONS

Configuration	M_∞	δ_F, deg	α, deg	$pd/2V_\infty$	Re/ft x 10^{-6}	I_x x 10^3 ft - lb - sec^2
$B_S N_{S2} A_{S1} F_{S5}$	0.3	0	-0.13 to 24.00	0 to 0.14	2.2	2.175
	0.5		-0.11 to 24.04	0 to 0.08		
	0.8		-0.14 to 24.24	0 to 0.05		
	0.9		-0.13 to 24.25	0 to 0.06		
	1.2		-0.13 to 24.35	0 to 0.05		
$B_S N_{S2} A_{S1} F_{S5}$	0.3	3	-0.13 to 24.00	0 to 0.04		2.217
	0.5		-0.13 to 24.10	0 to 0.04		
	0.8		-0.14 to 20.22	0 to 0.04		
	0.9		-0.14 to 24.17	0 to 0.04		
	1.2		-0.13 to 24.34	0 to 0.04		
$B_S N_{S2} A_{S2} F_{S5}$	0.3	3	-0.13 to 23.96	0 to 0.05		2.108
	0.5		-0.14 to 24.01	0 to 0.05		
	0.8		-0.14 to 24.16	0 to 0.05		
	0.9		-0.15 to 24.28	0 to 0.05		
	1.2		-0.14 to 24.33	0 to 0.06		

UNCLASSIFIED

Security Classification

DOCUMENT CONTROL DATA - R & D

(Security classification of title, body of abstract and indexing annotation must be entered when the overall report is classified)

1. ORIGINATING ACTIVITY *(Corporate author)*

Arnold Engineering Development Center
Arnold Air Force Station, Tennessee 37389

2a. REPORT SECURITY CLASSIFICATION

UNCLASSIFIED

2b. GROUP

N/A

3 REPORT TITLE

TRANSONIC AERODYNAMIC CHARACTERISTICS OF BOMBLET MUNITION MODELS USED IN THE EVALUATION OF THE ROLL-THROUGH-ZERO AERODYNAMIC DISPERSION TECHNIQUE

4. DESCRIPTIVE NOTES *(Type of report and inclusive dates)*

Final Report - January 4 to April 20, 1972

5. AUTHOR(S) *(First name, middle initial, last name)*

T. O. Shadow and G. R. Gomillion, ARO, Inc.

This document has been approved for public release
its distribution is unlimited. Per TAB 72-1
2 6 march 1972

6. REPORT DATE	7a. TOTAL NO. OF PAGES	7b. NO. OF REFS
July 1972	67	8

8a. CONTRACT OR GRANT NO.	9a. ORIGINATOR'S REPORT NUMBER(S)
b. PROJECT NO 2547	AEDC-TR-72-106 AFATL-TR-72-138
c. Program Element 62602F	9b. OTHER REPORT NO(S) *(Any other numbers that may be assigned this report)* ARO-PWT-TR-72-90
d.	

10. DISTRIBUTION STATEMENT Distribution limited to U.S. Government agencies only; this report contains information on test and evaluation of military hardware; July 1972; other requests for this document must be referred to Air Force Armament Laboratory (DLDL), Eglin AFB, Florida 32542.

11. SUPPLEMENTARY NOTES	12. SPONSORING MILITARY ACTIVITY
Available in DDC	AFATL (DLD) Eglin AFB, Florida 32542

13 ABSTRACT

A wind-tunnel investigation was conducted in the Aerodynamic Wind Tunnel (4T) to determine the aerodynamic characteristics of bomblet munition models designed for the evaluation of the Roll-Through-Zero Aerodynamic Dispersal Technique. Static stability pitch-damping, roll-damping, and magnus data were obtained at Mach numbers from 0.3 to 1.2 and angles of attack from zero to 24 deg at a constant Reynolds number of 2.2×10^6 based on the model length. Roll angle was varied from -165 to 180 deg for the static stability phase.

DD FORM 1 NOV 65 1473

UNCLASSIFIED

Security Classification

14. KEY WORDS	LINK A		LINK B		LINK C	
	ROLE	WT	ROLE	WT	ROLE	WT
ammunition						
bombs (ordnance)						
aerodynamic characteristics						
transonic flow						
wind tunnel tests						

AFSC
Arnold AFS Tenn